# Application of Electrical Resistivity Tomography (ERT) and Arial Photographs Techniques in Geo Hazard Assessment of Karst Features in Constructing Sites in Perak, Peninsular Malaysia

Riyadh R. Yassin*, Ros Fatihah Muhammad, Samsudin Hj Taib

Department of Geology, Faculty of Science, University of Malaya, 50603 Kuala Lumpur, Malaysia. *Email:
riyadh.geophsea@gmail.com

**Abstract**

This paper illustrates the application of geophysical survey, aerial photographs and satellite images as identification techniques for geohazard assessment of karst features in housing complexes construction sites north of Ipoh city, Perak state, Peninsular Malaysia. The engineers in Perak face numerous problems while designing structures that would be situated over marbleized limestone (carbonate) karst terrains, due to its categorization to various bedrock solution features such as sinkholes, caves, cavities, depressions, conduits enlarged joints and fractures, and internal drainages, which directly exerts a negative impact on the use of this land for construction projects and structures. Furthermore, it can also indirectly have the potential to cause catastrophic damages in the near future perhaps many years after the project has ended. The subsidence damages which result in construction works will cause massive losses which maximize the project overall cost leading to enormous financial costs, to the developers and the lands. In this study, Two-dimensional (2D) electrical resistivity tomography (ERT) survey was performed across three housing complex construction sites north of Ipoh in order to image the subsurface and locate evidence for near surface karstic features such as voids or cavities, including sinkholes and to estimate the depth of the bedrock. It is also done in order to estimate whether geophysical techniques are capable of identifying such features. Six resistivity traverses or profiles were conducted along the survey area at each of the three construction sites. The orientation, extension and the degree of inclination of those profiles are shown in Google's satellite map. The interpretation of the geophysical data indicated that both low resistivity and high conductivity anomalies extends along the proposed area in all of the construction sites. The ambiguous anomalies observed in construction site # 1 indicated that the area has been exaggerated by a sinkhole, thus it contains non-stiff clay and is saturated with water, rendering it less resistant to electrical currents (high conductivity). The ambiguous anomalies observed in construction site #2 indicated that the area has been affected by several sinkholes and tubular anomalies containing both stiff and sandy clay. The anomaly observed in construction site #3 indicated that the area has been affected by several soil cover collapse sinkholes and tubular anomalies containing stiff, non-stiff and sandy clays. This study also demonstrated that high-resolution Electrical Resistivity Tomography (ERT) can be effectively applied to reflect and differentiate surficial soil, clay, weathered rocks, compact or intact rocks, and air-filled karstic voids or cavities. The appearance of many sinkholes in the area is mostly attributed to karstic activity. In accordance to the classification of the characteristics of morphological features of karstic ground conditions by (A. C. Waltham and P. G. Fookes, 2005), the karst in construction site site#1 found between profile 1 and profile 6 is an older or complex karst type KIV, while the karst in construction site#2 found between profile 1 and profile 3 is a youthful karst type KII. Afterwards, the karst type changed over profile#5 to profile #6 to mature into karst type KIII. The karst in construction site#3, found between profile 1 and profile 3, is a youthful karst type KII. Then, the karsts change in profile 4 to an older, mature karst type KIII. The karsts found between profile #5 and profile#6 is of the older or complex karst type KIV.

Early planning is needed to mitigate or minimize the risk of structures in these construction sites over karstified carbonate bedrock. Initial consolidation of geo grids, driven piles to rock head pinnacles, and control drainage works must be put into operation in these respective sites.

**Keywords:** Application, ERT and arial photographs Techniques, Geo hazard Assessment, Constructing sites, Perak- Peninsular Malaysia.

## 1. Introduction

The location and condition of carbonate bedrocks such as limestone or marbleized limestone and its appearance is important for engineering construction work, such as buildings, housing complexes and roads projects in Ipoh, which overlays Kinta marbleized limestone. Sinkholes can cause construction delays and stability problems, which may amplify the cost of the project due to possible wall cracking, collapse of buildings' foundations, or subsidence and cracking on paved roads. These are only a small amount of examples of problems associated with sinkholes, karstic cavities and voids. Structural instabilities associated with these features can arise as a result of sudden collapse of the ground surface or as a less catastrophic but recurring drainage problem. Within

karst regions, the design and execution will be expensive vis-à-vis present and future structures. Moreover, borings that are drilled within karsts regions do not overlap areas of concern on the subsurface. Inappropriate and mismanaged borings are incapable of providing ample subsurface data for analysis, and at the same time, can also misrepresent the subsurface system, which may lead to additional costs for corrective design or additional analysis. Rapid reconnaissance surveys using satellite images and surface geophysical techniques incorporated into a boring plan are the best obtainable options that can be used to aid in suitable location of test borings in identifying or distinguishing the subsurface features related to karst development.

The 2D resistivity imaging technique was preferred for subsurface investigations over other geophysical methods for its high contrast or disparity in resistivity values vis-à-vis the different types of sediments, such as stiff or non- stiff clay, soil, sand, air or water in-filled cavity or voids, compared to the bordering or surrounding marbleized limestone bedrock. These entire elements reflector reproduce the use of resistivity imaging method that outlines and delineate the boundary between bedrocks and overburden layers. Moreover, this method is manageable with respect to time for small-scale projects in both pre and post-ability processing steps, rendering it the most appropriate for this type of investigations.

Electrical resistivity tomography surveys were functional at three constructions sites north of Ipoh. Construction site #1 is located at Klebang Putra - Klebang Green, and Construction site #2 is located at Medan Klebang Restu-Klebang Damai, north of Ipoh, while Construction site #3 is located at the north of Bandar Baru Putra. Figure 1 highlights the locations of the studied construction sites in Kinta valley, north of Ipoh, Perak, Malaysia.

**Figure 1: Google satellite images viewing the locations of studied construction sites in Kinta valley, north Ipoh city, Perak state, peninsular Malaysia**



## 2. The study objective

The objective of this survey is to:

    I.     Determine the subsurface in order to locate evidence for near surface karstic features (voids or cavities) including sinkholes, and whether clay or air-filled karstic voids or cavities are present in the subsurface.

    II.     Estimate the depth of the marbleized limestone bedrock.

    III.     Estimate the depth, shape, type and understand the origin of these karst features.

    IV.     Produce the geological model to represent the study area.

V.     Evaluate the subsurface structure levels and extent that can result in potentially dangerous collapse or ground failures at construction sites that superimpose these features.

VI.    Identify subsurface conditions that might compromise the reliability of any proposed future work in these sites, for example, an inactive sinkhole in-filled with thick clay. Under-compacted clay could present a critical problem, as the clays could accumulate under load, resulting in leakages all the way down to the bed rock.

VII.   The best solution methods frequently used in the plan to minimize the risk of problem areas in these construction sites.

## 3. Geology of the study area

### 3.1 Topography and geomorphology of study area

Kinta Valley is a triangular-shaped or V-shaped valley bounded by the Main Range on the east, which is rises to 867 m above the mean sea level and Kledang Range in the west. The northern tip of the triangle starts at around Chemore town in the north. The valley in this region broadens to about 7 km, and broadens in the south around Kampar town to reach this region, at about 20 km. This valley is extended over a distance of 45 km from north to south. The first tower karst observed in Kinta Valley is Gunung Kanthan in the north, and the last is Gunung Tempurung in the south.  The alluvial plain is situated at about 60 m to 80 m above the mean sea level.  This is an area that has seen active tin-mining activities, and most of the tower karst and subsurface karst remains exposed.

Major rivers originating from the granitic Main Range highland drains into most of the karstic land in the study area. The famous one drained to Kinta Valley is Sungai Kinta; extending from the northeast down to Bota in the southwest to meet Sungai Perak. Major tributaries of Sungai Perak that drains into the valley and run through the limestone towers from the east and northeast of the valley are Sungai Pinji, Sungai Raia, Sungai Dipang, Sungai Kinta, Sungai Tempurung and Sungai Kampar. Those tributaries transport alluvial deposits to the eroded marbleized limestone, creating a flood plain across the low-lying valley.

### 3.2 Geology Age of Kinta Valley

Kinta Valley, located in western Peninsular Malaysia, forms a V-shaped valley that opens to the south, and is bounded by the granitic massif of the Main Range to the east, and of the Western or Kledang Range to the west. The granite that forms the mountains was determined to have been formed during the Triassic age (Cobbing et al, 1992).

Geologically, most of the study area is underlain by Kinta's limestone, whose origin was pinpointed to be somewhere between the Devonian to Permian periods (Suntharalingam, 1968). Most of the limestone is found beneath the general surface, where it is covered by Tin- bearing alluvium, which gave Kinta Valley its moniker of 'mining town', dating all the way back to the previous century.

The mogote or isolated residual limestone hills that are seen in the Kinta Valley constitute less than 10 % of the actual surface of the limestone bedrock that occurs in Kinta Valley (Ros Fatiha, Yeap Ee Beng 2003).

The Schist layers that are found underneath to be interbedded with limestone are in Kinta Valley. In terms of age, it is probably younger, however, most of it could be older than Devonian. Both the limestone and schist were probably formed at the end of the Permian period. They also undergo metamorphosis at the same time, forming mainly quartz-mica schists and the fine-to-medium to coarse-grained white to dark-grey calcitic marble, with some minor black and reddish coloured dolomites.

The limestone hills extend 20 km north of Ipoh and 20 km to the south. Due to the surrounding karst formations, there are many limestone karst caves in these hills;

Cave temples are built into some of these caves, while others are show caves accessible to the public, for example the Gua Tempurung cave near Gopeng, south of Ipoh, which is the largest and deepest cave in Peninsula Malaysia.

The surface geology of Ipoh area is well documented by Yin (1976) and Ingham & Bradford (1960). Table-1 summarizes the geology and stratigraphy of the study area. The limestone bedrock in the area rises above the alluvial plains to form limestone hills with steep to vertical slopes (mogote or tower karst). Flanking the limestone on the eastern and western sides of the valleys are granitic uplands. This geological setting has given rise to alluvial deposits that are rich in tin – hence, the growth and development of the area as a "mining town" since the previous century.

The eastern part of the area is comprised of limestone hills formed during the Silurian to Permian periods, which has mostly metamorphosed to marble. The limestone hills that were discovered are covered by a huge amount of vegetation. The outcrop of limestone hills can be found to be widespread on the eastern part of the study area.

**Table 1: Geology/stratigraphy of the Ipoh areas after (Yin, 1976)**

| No. | Age of sediment | Type of sediment in the study area |
|-----|-----------------|-------------------------------------|
| 1. | Quaternary | Alluvium (Young and old alluvium) |
| 2. | Triassic | Granite & Allied Rocks |
| 3. | Palaeozoic | Kinta Limestone (dominant) <br> Basal Schist |

The subsurface geology of Ipoh is predominantly important for any construction projects, especially for high-rise buildings. Numerous construction projects in the area, either through data from numerous boreholes, or definite excavations, have determined the typical subsurface geologic features and soil profiles of the urban area, (Ingham & Bradford, 1960) and (Yin, 1976). For example, limestone bedrock and its association with karstic or dissolution are featured as highly irregular in limestone bedrock profiles, steep cliffs of pinnacle, solution channels and caves and cavities, arches, and overhangs, etc, which are major concerns to the local foundation engineers construction projects.

The subject of foundations over limestone bedrock in Ipoh was the subject of quite a few studies. A review of borehole data by (Tan, 1988) showed that the depth to limestone bedrock in the Ipoh area is generally less than 20 m. The review of the borehole data also showed the size of the cavities in the limestone bedrock were mostly < 3 m across. Yassin, 2009-2010, applying the E R Tomography geophysical technique in 17 sites of different construction projects in and around Ipoh pointed out that the surface of marbleized limestone bedrock was uneven and contain numerous pinnacles and cutters. The depth of marbleized limestone bedrock ranged between 3 m to more than 28m in the site. Also, the soil profiles in Ipoh area are comprised of alluvium (fluvial deposits) and/or mine tailings, overlying the marbleized limestone bedrock.

### 3.3 Lithology of study area

In Kinta valley, the lithology of the study area is consisting of four main types, each resulting in a different landscape.  They are:

I. Carbonate rocks forming Kinta Limestone, where it has undergone tropical karstification to form steep sided and cockpit towers protruding across the enormous plain.

II. Granite bodies of the Main Range and Kledang Range (series) that flank the plain in the east and west, respectively, forming rugged ranges of up to 1000 m above mean sea level.

III. Schist, which makes up the rolling landscape of the valley.

IV. Quaternary alluvial deposits that has been deposited across the valley and form an enormous plain.

**Figure 2: Geological map of Kinta valley viewing the location of construction sites under study North of Ipoh city, Perak state**
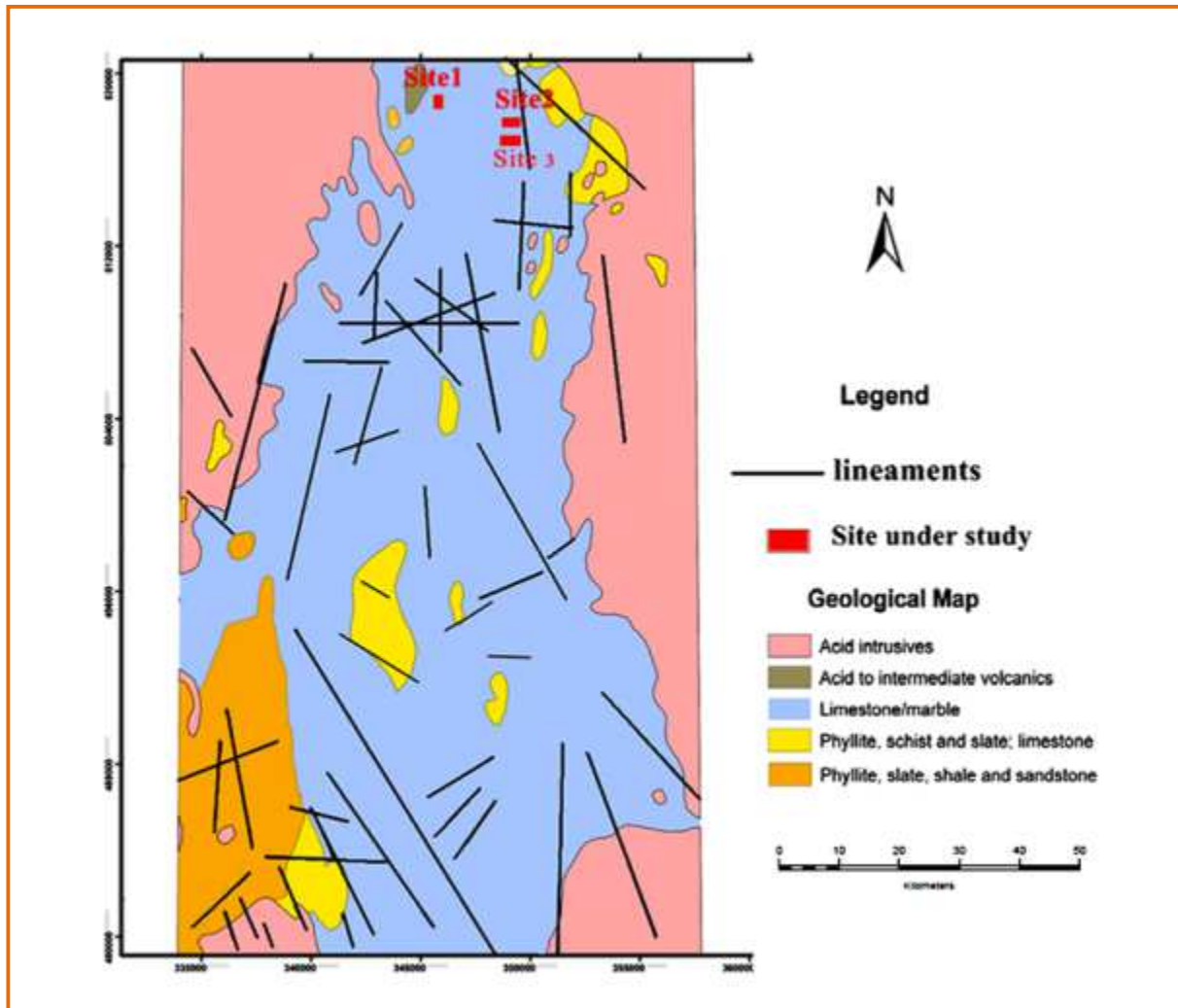


### 3.4 Development of the karst phenomena in sungai Perak basin (Kinta valley)

Many geologists have suggested that major karstification is controlled by the structures in the areas where it occurs. The structural geology in the limestone of Kinta valley are dominated by faults and folds oriented north-south, which results in a noticeable grain to the landscape, especially to the orientation of (mogotes) isolated, steep-sided, residual, and hills, which are composed of either limestone, marble, or dolomite, and surrounded by nearly flat alluvial plains in the central part of the valley. Vertical and sub-vertical joints and faults in the marble are its main lines of weakness. The subsurface karst is characterized by the formation of rounded top pinnacles and irregularly shaped sinkholes, which had previously been referred to as dolines.

Rainfall containing dissolved carbon dioxide results in a strong acid identified as carbonic acid ($H_2CO_3$). It will get more acidic as it filters through side soil, as there is more carbon dioxide residing in the gaps in the soil – up to 100 times more than what is in the atmosphere. The authors believe that the most imperative recent thought is the fact that enhanced rainfall and elevated acidity of the rain in the last few decades of the 20th and 21st century in Malaysia and other countries in South East Asia are due to the dramatic increase in the amount of liquefied carbon dioxide.

These are mostly caused by volcanic and tectonic activity in the Pacific fire ring, with volcanoes in Indonesia and Philippines being the most active. A spectacular submarine volcanic eruption spews out huge columns of ash, smoke, gases and vapours thousands of feet into the Pacific Ocean's sky. Land clearing activities such as those practiced by Indonesia on a large scale also results in the emission of large volumes of pollutants into the atmosphere. Vehicular and factory emissions are also significant contributors to air pollution. All of these events have a large impact on the development and quick dissolving process of carbonate rocks. The authors also

believe that most of the biggest cave and channels in the limestone of Kinta valley are due to the reaction of sulfuric acid (H2SO4) with carbonate rocks, and can also be one of the corrosion factors in karst formation; this mechanism may also play a role, as O2-rich surface waters seep into the ground, carries oxygen that which reacts with sulphide, which are present with Cassiterite into the ground surface of Kinta valley area. The oxidation of sulphide leads to the formation of sulfuric acid. Sulfuric acid then reacts with calcium carbonate, causing increased erosion within the limestone's formation.  The cover layers of alluvial deposits over marbleized limestone of Kinta valley contain soil-piping or channels features. The Tin (Cassiterite) accumulates in this alluvial channels or pipes, having been washed down from the granite ranges and carried by rivers as previously mentioned, which contain sulphur in its chemical deposits, having a large impact on the development and quick dissolving process of carbonate rocks.  Furthermore, replacement deposits, consisting chiefly of Cassiterite and sulphide minerals deposits are found in replacement pipes in the Kinta Valley area, which replaces dolomitic or calcareous sediments.

## 4.    Hazards of soil-cover karst collapse

The collapse of soil-cover karst most often occurs in Perak region having the most active karst features. It occurs in areas of dolomitic or marbleized limestone bedrock, which locally has little to no surface evidence of features related to subsurface karst. The early stages of a soil-cover karst collapse may appear as a soil-piping feature, but can rapidly turn into a potential threat for the subsurface structure. The pre-collapse field conditions disclose little evidence of subsurface karst. The geological characteristics common to most collapse locations are groundwater that are ≥15 m below the surface, soil materials subjugated by porous layers, residual silty-clay soils with relict bedrock structure of ≥ 9m thickness, highly weathered condition of underlying limestone or dolomite bedrock, or positions close to active sinkholes or within a loosened stream valley. The soil cover collapse in the Perak region is mostly due to the cover layers of alluvial deposits over marbleized limestone of Kinta valley containing soil-piping or channels features. Several factors are directly related to the collapse occurring, including descriptions of overburden, depth to groundwater, geologic setting of the area, types of weather and karst development. These factors must be recognized, calculated and standardized in order to be utilized in an analytical method, which include measuring and normalizing the geological outcrop patterns, and identifying the ground water that interconnect the karst features and structural features of the area.

The sudden appearance of a soil cover collapse sinkhole is initiated when the development of small voids at depths of a few meters in soil or unconsolidated cover overlying karstic bedrock are enlarged by a loss of cohesion or loading of the arch-forming material caused by either saturation of the soil by rainwater precipitation or by rapid draining of a submerged void, which also increases pore pressure. This results in a loss of strength in the arch, making it too thin to support its own weight. This causes the underside of the arch cracks down into the void.

## 5.    Engineering classification of karst ground condition

The dissolution of carbonate rocks such as limestone, dolomite and marbleized limestone by natural waters creates extensive karst landforms that are problematic for civil engineers. Karst features develops on soluble rocks, both at the surface and subsurface, due to the rate of dissolution processes, which depends on a number of factors, such as the power of rainfall, availability of surface water, and its form of revive as well as groundwater, distribution of soil-cover, temperature and biological activity, the diffusion rate, autogenic content, structural weakness and the lithology of the carbonate sub layers.

Sinkholes were mostly created on soluble carbonate rocks (limestone, dolomite, dolomitic limestone and marbleized limestone). Sinkholes develops at both the surface and subsurface, due to the dissolution related to the difference in composition and associated processes, and pose many problems, which are classified A. C. Waltham and P. G. Fookes, 2001 into six types, including the type subsidence sinkholes that forms in soil cover within karst terrains.  Sinkholes have a wide-ranging destructive effect on many regions in the world. The creation of sinkholes may cause severe damage to man-made structures, and may even be a hazard to human lives if it occurs in a catastrophic way.

Voids in bedrocks can hinder surface-water flow and disrupt the surface drainage system. Soil and other surface material may be washed into the underground network of cavities. Sometimes, less tangible karsts can significantly influence water quality. Caves threaten foundation integrity when the width of the cave is greater than their roof's thickness. The networks of consistent caves and voids allow contaminants such as sewage, landfill leachate, or hazardous chemicals to travel unimpeded into shallow aquifers that may supply drinking water. The issue of the probable presence of solution features must be cautiously considered while making land-management decisions, including decisions that involve protecting water supply, locating septic systems, and placement of waste disposal facilities. Rock head creates difficult ground to excavate, and are found with varied morphology; from uniform to relief pinnacles.  The engineering classification of karst ground conditions by A.C.

Waltham and P.G. Fookes, 2005, is based on features that occur on the intact carbonate rock, and characterizes the karst in terms of the complexity and difficulty to be encountered by the foundation engineer.

### 5.1  Identification of sinkholes and subsidence areas by applying geophysical technique

The assortment and application of geophysical techniques intended to reduce the risk of sinkhole formation generally require the detection of existing sinkholes and the explanation of the areas where unique sinkholes are most likely to occur in the future. It is also imperative to gather information regarding the size and the frequency of the sinkhole events, subsidence mechanisms, and rates. However, it is usually a tedious task to identify the areas affected by carbonate dissolution subsidence. Sinkholes are usually enclosed by human activities, such as filling and development, or natural attrition processes may well eradicate them.

Generally, sinkholes may have a very fine geomorphic appearance, as the collapse produced by the underground processes may have yet to reach the ground surface. Many sources of surface and subsurface information need to be examined to gather sufficient data regarding the past and existing subsidence movement in the study area. In order to partially address these difficulties, the geophysical examination techniques can be used to detect the changes in the physical ptroperties and the anomalies of the ground that is connected with air-filled, water-filled or sediment-filled cavities, breccias pipes, subsidence of structures ravel zones, synclinal hang down, down thrown blocks, irregularity of rock head topography and covered sinkholes. Major characteristics of the ambiguities must be acknowledged for certain interfering methods such as excavating trenches, borehole drilling or applying of borehole probing.

There are a multitude of methods whose applicability and fitness depends largely on the investments available, type of necessary deposits, geological situation uncovered, the over covering or inter layers of the karsts, the topography of the area and the probable type of structures dissolution, the estimated type of structures subsidence, existence of interfere factors such as man-made services, and the required penetration and declaration. Sinkhole activity has become obvious in developed areas, especially via the deformation of roadways and buildings, intermittent services, and other formation. Applying geophysical approaches for mapping the subsidence destruction, information on the spatial allocation of the subsidence can be gained, and major natural and human factors that control the dissolution and subsidence processes may also be conditional. Devastation of buildings can also be recorded on performance evidence sheets for it to be converted and supplied to a GIS and database system.

The best option is to apply two or more geophysical techniques, and compare the results to each other. It is wise to apply the geophysical examination techniques on the sites prior to drilling as one of the phased sequences of investigation. The area with aberrations and the normal areas bereft of aberrations are recognized delineated, and planned for construction projects. Evaluation of geophysical techniques used in karst areas has been presented by Hoover (2003) and Waltham et al. (2005). A number of previous geophysical studies in the karst areas apply the (ERT) technique to map the bedrock surface, W. Zhou B.F. Beck J.B. Stephenson, 2000, a site in southern Indiana, where limestone is covered by about 9 m of clayey soils. Forty-nine profiles were created over an area of approximately 42,037 m2. The repeatability of the ERT technique was evaluated by comparing the previous drilling section, with the interpreted ERT section from pairs of transects where they crossed each other. To identify the depth of mud-filled void and its extension, William E. Doll', Jonathan E.  Nyquist, Philip J. Carpenter, Ronald D. Kaufmann, and Bradley J. Car-r', 2002, conducted geophysical surveys at a site on the Oak Ridge Reservation (ORR), Tennessee, USA. The data suggest that an optimal scheme for detailed karst mapping might consist of multi electrode resistivity surveying, followed by the joint inversion of gravity and seismic travel time data. The resistivity results could be used to produce an initial model for the seismic and gravity inversions. To identify buried sinkholes and other karst features in the zone of karst terrain, Kachentra neawsuparp and tanad soisa (2007) applied 2D and 3D resistivity imaging resistivity (ERT) survey at the Ban Pakjam in Huaiyod district, Trung province, southern Thailand. The 2D resistivity surveys clearly show the central depression, as well as resistivity contrasts between the cover sediments, delineating the in-filled sinkholes, underlying weathered bedrock, and map the locations of sinkholes in this covered karst terrain.

### 5.2  Identifying Sinkholes by Employing of Aerial Photographs and Satellite images technique

Large-scale colour stereoscopic aerial photographs are very helpful in identifying sinkholes. The key limitation of aerial photographs and satellite images is that, depending on the scale and explanation of the images, it may not be feasible to pinpoint small or shallow sinkholes.

**Figure 3: Five layers spot images of Perak state (2008) presenting the location of construction site #1, site #2 and site #3 north of Ipoh city (Kinta valley)**
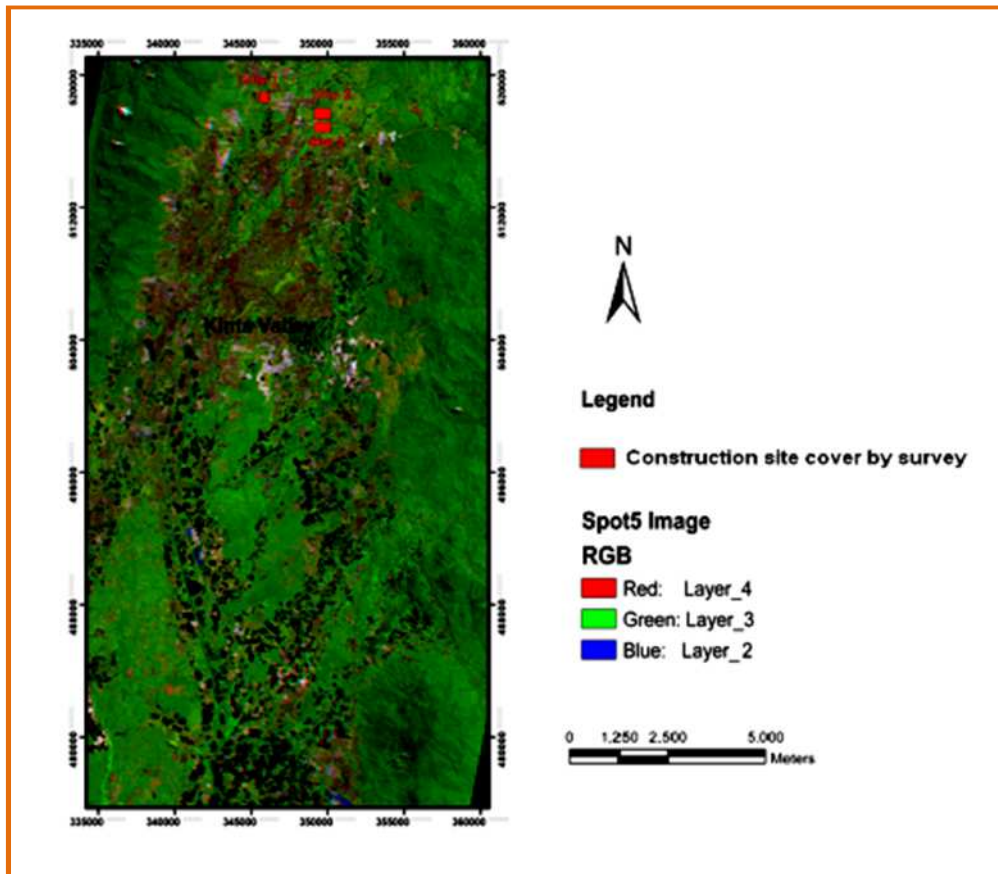


Old aerial photographs are usually very helpful in detecting sinkholes that are enclosed by buildings or man-made structures. The thorough elucidation of photographs taken on different dates allows the chronology of freshly formed sinkholes to be inhibited. The interpretations help to gain minimum estimates of the possibility of sinkhole occurrences, and permit the study of the spatial-temporal allocated patterns of the subsidence phenomena. The usage of low sun-angle photographs with apparent shadows emphasizes subtle topographic features.

The more advance technique is the investigation of airborne and satellite multispectral and thermal images, which may be used to distinguish the surface terrain patterns and acquire variations in moisture, vegetation, colours, and heat related to subsidence areas and sinkholes. In this current work, usage of satellite images of Perak is on the scale 1/5000 of year (2008). Additionally, Global Position System (GPS) and Geographic Information System (GIS) technologies have immensely improved examinations. The common methods of mapping land and utilizing changes are typically high in cost and low in precision. The remote sensing provides updated information on land by using these methods. Natural events and human factors can also be observed by using current and archived distantly sensed data.

**Figure 4: land Photographs viewing several positions that recognized in aerial photographs in construction site #1, which identified as the depositional of gry swamps clay**



The interpretation of the aerial photographs of the study area and its surroundings to determine the fracture system, topography, and drainage pattern was conducted. These old aerial photographs were operational in 1965 under the Colombo Plan, possessing a scale of about 1: 25,000. Table 2 shows the list of aerial photographs used in this study. The technique for this aerial photographic interpretation of the karstic features, such as limestone isolated residual hills (mogotes) and the cliffs, and also the lineaments, forests, and plantations. The significance of the karstic features and their possible origin in relation to the geological features are concluded as well. Also, the interpretation showed that the orientation of lineaments from the Main Range and Kledang Range is far from irregular, but shows the dominant strike of northwest to Southeast, with a subsidiary set striking east-northeast to west-southwest. It was concluded that these lineaments were also observed to be clearly cutting the marbleized limestone of Kinta valley and the hills above it. Figure 3 shows the direction of the lineament in the study area that are taken from the aerial photographs, satellite images, and setting on geological maps. The drainage in this study area is rather straight and angular, and aerial photographs show that stream courses are controlled by the direction of lineaments (joints, fractures and fault systems) in the marbleized bedrock. In addition, the aerial photographs show that the area of construction site #1 was a swamp area with bushes. The aerial photographs also shows that the area of construction site #2 and site #3 were covered with forest, and some parts with oil palm plantations. Furthermore, the satellite images' shows that part of the forest in site #1 were removed for the construction project. Moreover, it was determined that isolated residual limestone hills were distributed in the south and south west of construction sites #2 and #3, respectively.

**Table 2: Presenting the list of aerial photographs which employed in this study**

| Location | Roll no. | Line no. | Print no. |
|----------|----------|----------|-----------|
| **Ipoh** | C-12-A | L32N | 20-30 |
| | C-6 | L31N | 20-55 |
| | C-5 | L30S | 80-90 |
| | C-5 | L29N | 120-125 |

### 5.3 Reconnaissance field surveys

Direct ground inspections in the two construction sites resulted in the discovery of sinkholes that were not visible in aerial photographs and satellite images due to many factors. For example, the area may be enclosed by vegetation, sinkholes definite size, or their depth is too small to be detected. The recorded model is used for the explanation of each sinkhole, including a diagram of the sinkhole and its access geometry, the covering features with the district and the coordinates, orientation, dimensions, age, continuation degree, vegetation and symbols of volatility as cracks, scarps or pipes. These features supply information on the activity and the periods of the sinkholes, and act as indicators of plausible location of future sinkholes in proximity to human structures and other observations. The existence of features such as muddy areas, or the expansion of vegetation and holes crammed with materials may help detect shallow subsidence depressions. Generally, the application of geophysical surveys is desired to determine whether these irregular characteristics are interrelated to sinkholes.

Ground inspection at site#1 reveals no sinkhole. On the other hand, aerial photographs of the area imply that it is made up of old swamps, which might contain sinkholes on its subsurface. More than four big black spots were recognized in aerial photographs, three of them circular to semi circular in shapes, while the others possess an extended shape. However, due to human activity and excavating work being done there as an ex–mining area, most of these features were packed with sand and other material, and among them, three areas with deposits of grey swamp clay in circular shapes were acknowledged. The clay seems to sink down due to numerous factors, which will be explained shortly. Figure 6 shows land photographs and the positions of three big black spots in the aerial photographs, which might include sinkholes under the depositional of gray swampy clay construction site #1

This area is identified and demonstrated as an area that might include a medium to large sinkhole, extended in the subsurface along this site of visually uncertain depth. This might point to the presence of clay or water in-filled karstic sinkhole or cavities that could compromise the probity of this site.

During the ground inspection at site #2, two sinkholes was discovered, but not recognized in aerial photographs and satellite images, as adjacent small plants enclose it. One of these sinkholes has a diameter of ~7m-10m., water in-filled, of visually undetermined depth, are recognized and proven as a sinkhole with a narrow showing throat, positioned in the south west flank of this site. The other sinkhole has a diameter of ~35m- 40m, positioned in the north east side of this site, was in-filled with wet clay and other material of sediments due to karst activity, raised a question that this sinkhole might be linked in the subsurface to one or more of the large tabular conduits or channels, and the presence of cavities or voids of undetermined depth. Clay, or air in-filled karstic sinkhole or cavities were present, which could compromise the veracity of this site. The south section of this site is littered with soil cover collapses.

**Figure 5 : Land Photographs viewing a number of sinkholes that identified as water in-fill, empty and covered with vegetation was determined as small and narrow in construction site #2 and site#3**



## 6. Location of study area

### 6.1 Construction site #1

Site #1 is situated at Klebang Putra – Klebang Green to the north of Ipoh city (Kinta Valley). It is situated at latitude N4°41'0.96"-N4°41'26.96", longitude E101°05'55.68"-E101°06'21.6" as shown in Figure 6. It is located to the north of the main series, and east of the Kledang series. The project plan estimating constructing housing complex include 100 two floor linked houses, 50 bungalow houses and its facilities.

**Figure 6: Location Map, Satellite Images and land photograph viewing the location the study area in construction site #1**



### 6.2 Construction site #2

Site #2 is situated at Medan Klebang Restu- Klebang Damai to the north of Ipoh (Kinta Valley), positioned approximately at latitude N4°40'35.04"-N4°41'0.96", longitude E101°07'52.32"-E101°08'18.24", as shown in

**Figure 7: Location Map, Satellite images and land photograph viewing the location the study area in construction site #2**
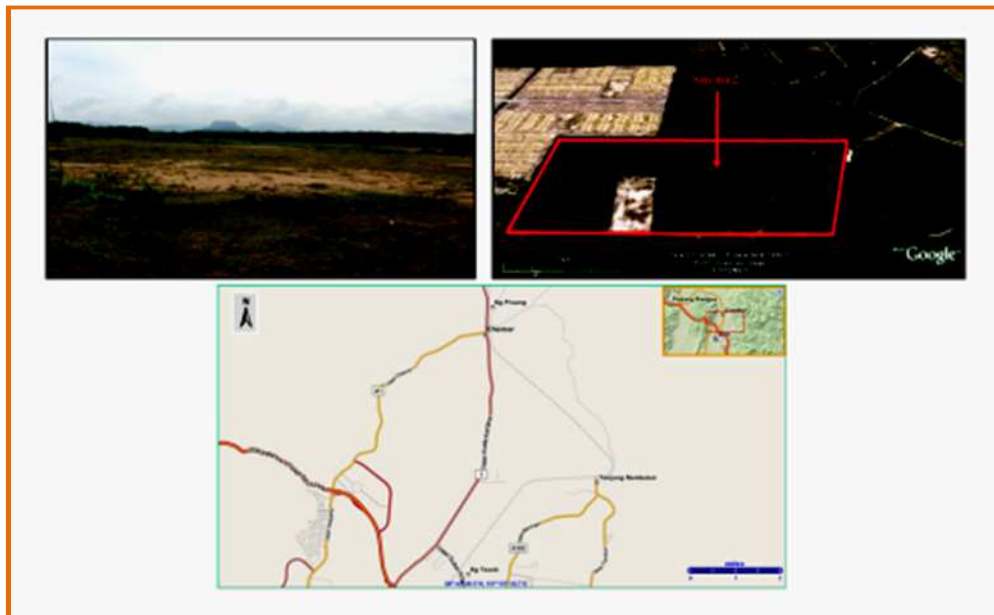


### 6.3 Construction site #3

Site #3 is situated north of Bandar Baru Putra, which is itself north of Ipoh (Kinta Valley), Positioned approximately at latitude N4°40'37.10"- N4°41'17.48", longitude E101°07' 51.77"- E101°08'08.33'', as shown in Figure 8. It is located to the west of the main series of Cameron Highlands. The project plan estimating constructing housing complex include 150 two floor linked houses and its facilities.

**Figure 8: Location Map, Satellite images and land photograph viewing the location the study area in construction site #3**
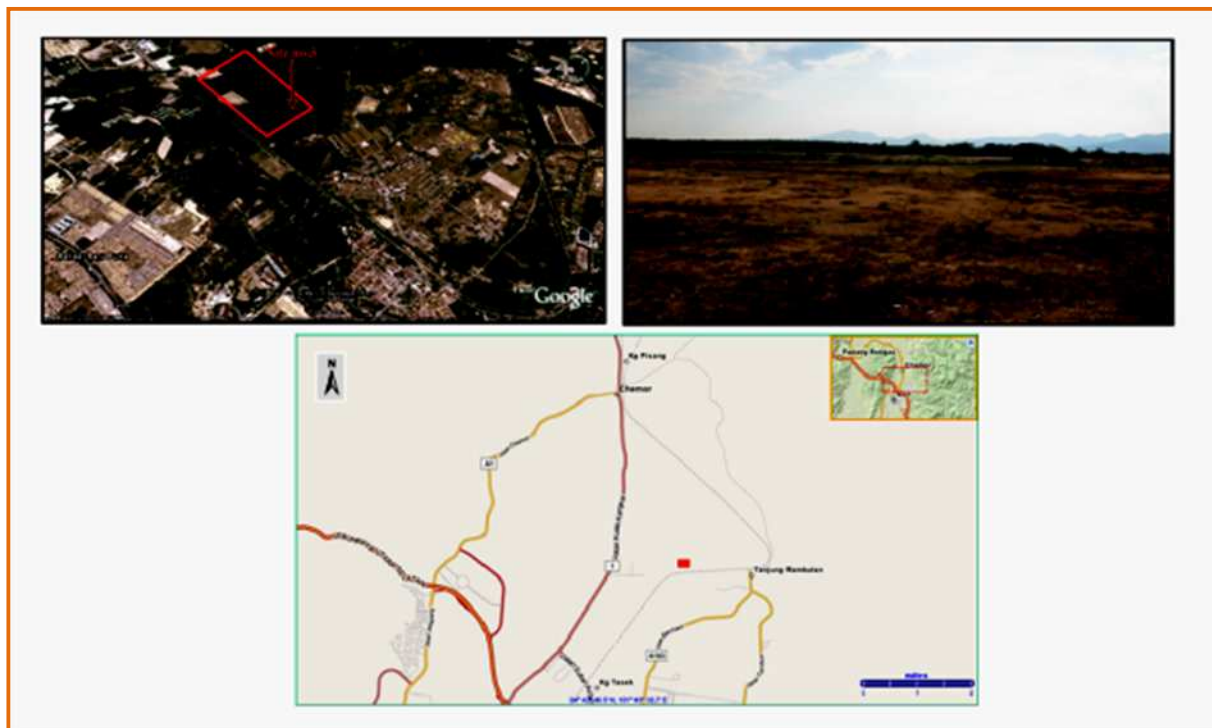
## 7.  Field survey technique
### 7.1 Instrumentation and measurement procedure

The survey was conducted using a SAS1000 resistivity meter, which has an inherent microprocessor that automatically selects the appropriate four electrodes for each measurement. The two dimensional (2D) - electrical imaging/tomography surveys are typically carried out by employing a large number of electrodes; 41, 61 and 81 electrodes along a straight line, coupled to a multi-core cable (Griffiths and Barker 1993), commonly at a constant spacing of 5m or 10m between the adjoining electrodes. When the succeeding measurements were taken, they were configured in a Wenner array and other survey parameters, such as the electrical current is usually converted into a text file, which can be read by a computer program. After reading the control file, the computer program then automatically detects the suitable electrodes for each quantity. A laptop computer was utilized to set the RES2DINV inversion software for the purpose of developing the resistivity model.

In a distinctive survey, most of the fieldwork involves laying out the cables and electrodes. After doing that, the measurements are taken automatically and stocked into the computer. This resistivity procedure usually gives a better grouping of spatial resolution and depth of study in karst terrain than any other geophysical technique.

**Figure 9: viewing the instrument type SAS1000 applied on geophysical survey**



### 7.2 Data collection

Electrical resistivity tomography (ERT) was used to image subsurface. The electrical resistivity data, composed along two dimensional (2-D) electrical resistivity profiles, were functional above and in proximity underneath, adjoining active and non-active sinkholes at two construction sites.

### 7.2.1 Data Collection in Construction site #1 (Klebang Putra)

Six electrical resistivity traverses or profiles, Profile-1 to Profile-6, were controlled over and along the survey area in site #1. The direction of these profiles in (N90ºW), and the level of those lines are shown in the location map, illustrated in Figure 10. The electrical resistivity data accumulated along the two dimensional (2-D) electrical resistivity profiles were determined to be in excess of, or beneath the sinkhole, using a 41-channel array in the Wenner configuration. The length of each profile was 200 m, with an electrode spacing of 5m, on average, spaced at 25m between each profile. The total length of all profiles in this site was 1200 m, covering an area of 30000 m2; 190 data points were composed for each (41-electrode) in one profile, and on average, about 1140 data were composed for a total six profiles in this site.

**Figure 10: Google earth satellite images viewing the location of resistivity profiles in construction site #1**
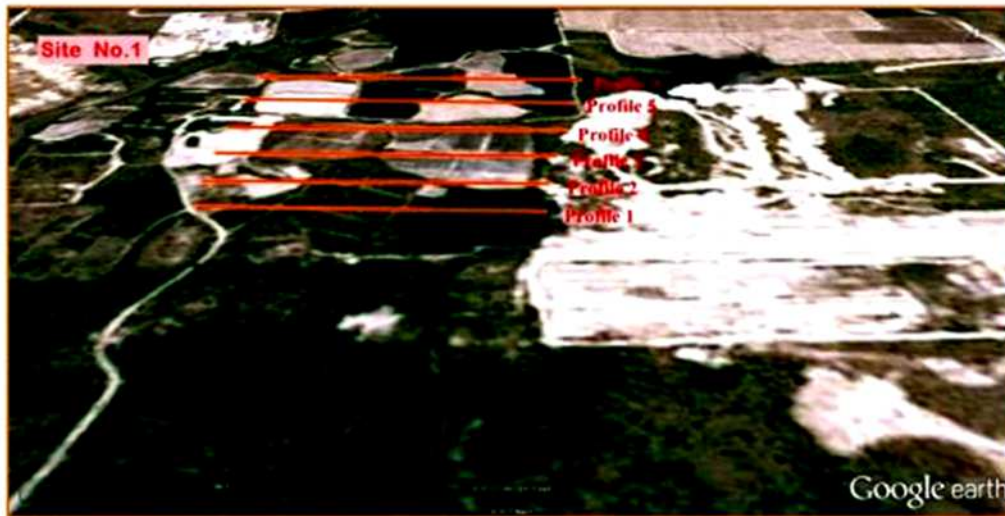


### 7.2.2 Data Collection in Construction site #2 (Medan Klebang Restu)

Six electrical resistivity traverses or profiles, Profile-1 to Profile-6, were conducted over and along the survey area in site#2. The directions of these profiles are in (N80º W), and the points of those lines are shown in the location map in Figure 11. The electrical resistivity data were acquired and accumulated for the purpose of mapping this site along the two dimensional (2-D) electrical resistivity profiles, in excess of, or beneath the sinkhole, using a 61-channel array in the Wenner design. The measurement length of each profile was 400 m, with an electrode spacing of 5m, on average, spaced at 25m intervals between each profile. The total length of all profiles in this site was 2400m, covering an area of 60000m2, and 320 data points were composed for each (61-electrode) in one profile. On average, about 1920 data were collected from a total six profiles at this site.

**Figure 11: Google earth satellite images viewing the location of resistivity profiles in construction site #2**



### 7.2.3 Data Collection in Construction site #3 (North Bandar Baru Putra)

Six electrical resistivity traverses, named Traverses-1 to Traverses-6, were controlled over and along the survey area at site #3. The directions of these profiles are in (N90ºW), and the levels of those lines are shown in the satellite image, illustrated in Figure 12. Electrical resistivity data were acquired and accumulated for the purpose of mapping this site along the two dimensional (2-D) electrical resistivity profiles, using an 81-channel array in Wenner design. The measurement length of each profile was 400 m, with an electrode spacing of 5m, on average, spaced at 25 m intervals between each profile. The total length of all profiles at this site was 2400 m, covering an area of 60000 m2, with 340 data points composed for each (81-electrode) in one profile. On average, about 2040 data were collected from a total six profiles at this site.

**Figure 12: Google earth satellite images viewing the location of resistivity profiles in construction site #3**
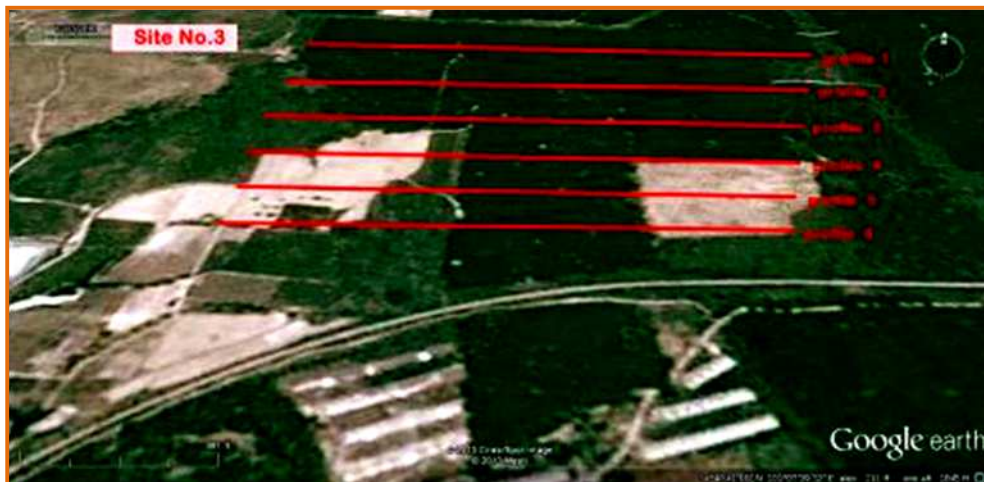


#### 7.3 Data processing:

After completing the field survey, the resistance measurements were regularly converted to apparent resistivity values. The data were developed to produce two-dimensional resistivity model of the subsurface. This step converts the apparent resistivity values into a resistivity model section that can be used to explain geological occurrences. The data were readily obtained in the RES2DINV formats, while the conversion program was outfitted with the system. The Root Mean Square (RMS) error statistics enumerate the distribution of the percentage differentiation between the logarithms of the calculated resistivity values, and those calculated from the true resistivity model (calculated apparent resistivity values). Data points containing errors of more than 30 % and above are usually omitted. In this survey, a small RMS value is indicative of the fact that less than 10% are defined by the convergence limit. The average default RMS error value in construction site#1 is 4.6 %, and the change in the RMS error between iterations was a minimum of 4.0%, and a maximum of 15.4%. The average default RMS error value in construction site#2 is 2.58 %, and the change in the RMS error between iterations was a minimum of 5.0%, and a maximum of 12.6%. The average default RMS error value in construction site#3 is 6.75 %, and the change in the RMS error between iterations was a minimum of 3.4 %, and a maximum of 9.7 %. To get a good model, the data must be of uniformly of good quality.

#### 8. Interpretation resistivity profiles

The ERT technique was applied in this geo-technical survey to investigate karst features such as sinkholes, cavities, depressions and channel pipes, For the reason that the tool is suitable for differentiating surficial soil, clay, sand, weathered marbleized limestone bed rocks, intact marbleized limestone bed rocks and water - air-filled cavities and channels. Also was applied due to its less relative effort and time effectiveness. It's based on the application of electric current into analyzed bedrock and measuring the intensity of electric resistivity to its conduit. Basically, it gives information of electric resistivity properties through the analyzed material towards electrical current passage.

Several reports and researches of application geophysical techniques in many karst terrains in several countries round the world were examined. These reports and researches are; "Assessment of Karst Activity at Highway Construction Sites Using the Electrical Resistivity Method, Missouri, USA" by Neil L. Anderson, Derek B. Apel and Ahmed Ismail, in year 2007. In addition The research of "Accurate Subsurface Characterization for Highway Applications Using Resistivity Inversion Methods "by Ioannis F. Louis, Filippos I. Louis and Melanie Bastou, in year 2002. Moreover the research of "Evaluating the presence of karstic Bauxitic clays in parts of Western Desert of Iraq by the application of VLF – electromagnetic and Electrical resistivity techniques" by Yassin R. Rafeeq, in year 2002.And the research of The research of " The application of complex geophysical techniques to detecting and locating the Weakness zone and the water seepage in the body of the AL-Tharthar dam , samara town, Salahuddin province / Iraq " by Niel A. Yahia , Yassin R. Rafeeq, Samer R. Hujab, in year1993. Enabled determination of the electrical variables associated with the nature of sediments. Deductions made based on the variations in electrical resistivity values with the nature of sediments of the study area. Hence, electrical resistivity values were determined for each rock unit.

Successful and defining imaging of the bedrocks and subsurface karsts features is appropriately suitable to provide geological classification based on the variations in electrical resistivity values of the study area into the surficial soil, clay, weathered marbleized limestone bed rocks, intact marbleized limestone rock, and air-filled

cavities. Clays are usually distinguished by its low apparent resistivities and variables, which are more dependent on moisture, mineral content, purity, and unit shape/size, usually from 5 ohm-m to less than 60 ohm-m, while sand is usually typified by low apparent resistivity and variables, depending on the moisture content, purity and unit size, usually from 70 ohm-m to less than 160 ohm-m. Comparatively weathered marbleized limestone rock is typified by high apparent resistivity that is typically more than 200 ohm-m to less than 400 ohm-m. Intact or unbroken limestone rock is distinguished by higher apparent resistivity, naturally more than 400 ohm-m to more than 4000 ohm-m, which varies depending on the layers' thickness, its impurities and its moisture content. Air-filled cavities or voids are generally characterized by very high apparent resistivities, classically >3000 ohm-m-6000 ohm-m, but varies depending on the conductivity of the nearby strata and the size/shape of void or cavity. Dolomitic limestone or dolomite with higher apparent resistivity, naturally more than 6000 ohm-m - 80000 ohm-m, varies depending on the layers' thickness. This will form the bulk of the work for electrical investigations survey in these sites for the purpose of understanding resistivity profiles. Hence, electrical resistivity values were resolute for each rock unit. The results are tabulated in Table 3. This table is useful in the context of investigating karst features and its deposits within carbonate karst terrains, while at the same time also being suitable for the purpose of detecting any mineral deposits within the sediments in the area, which requires extensive experience. In the following analysis, key explanatory interpretations were prepared for the geophysical electrical data in the selected study areas.

### 8.1 The interpretation of resistivity profiles in Construction site #1

The electrical resistivity data accumulated in this construction site was clarified in the deficiency of borehole control by applying Table 3 above. The interpretation confirms that a massive sinkhole is present at this site and is unmitigated, located between resistivity Profile #1and Profile #6.

**Figure 13: Inverse model of electrical resistivity section form profiles#1 to profiles#6, viewing the interpreted location of karst features (cavities and sinkholes) in Construction site #1**
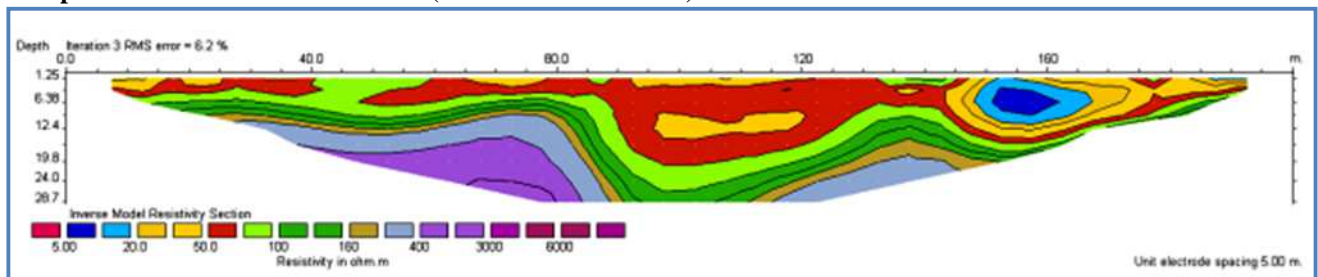


(Figure - A) Inverse model of electrical resistivity section for profile no. 1 (Klebang Putra)
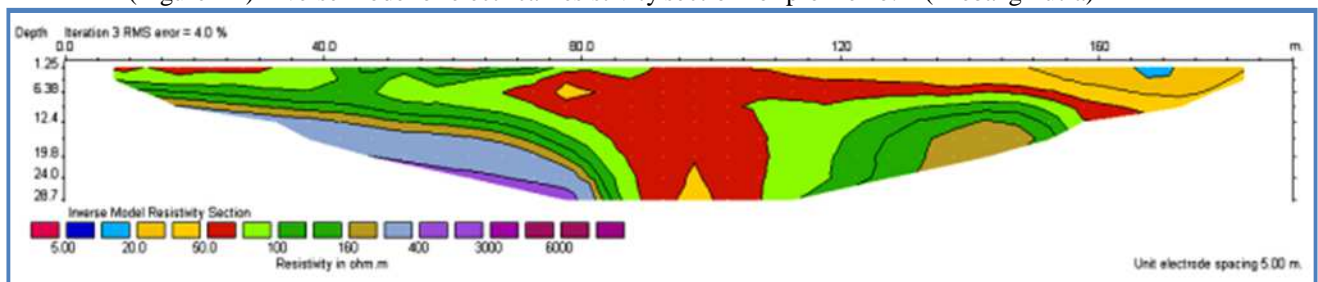


(Figure - B) Inverse model of electrical resistivity section for profile no. 2 (Klebang Putra)
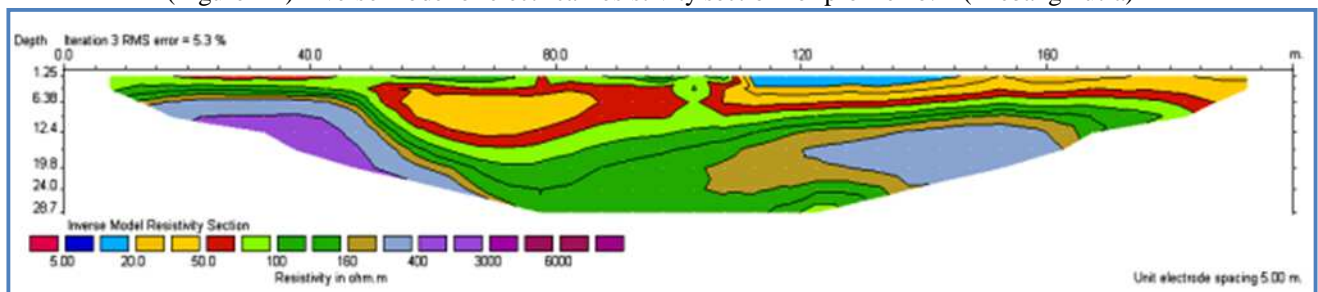


(Figure - C) Inverse model of electrical resistivity section for profile no. 3 (Klebang Putra)
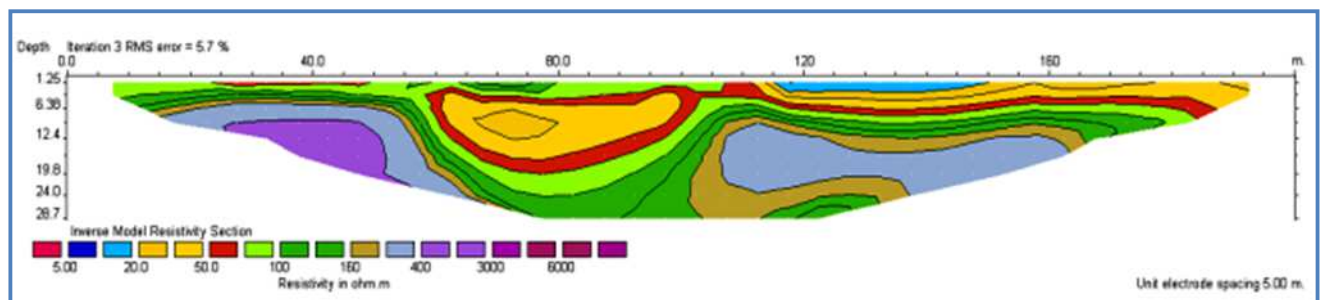
(Figure - D) Inverse model of electrical resistivity section for profile no. 4 (Klebang Putra)
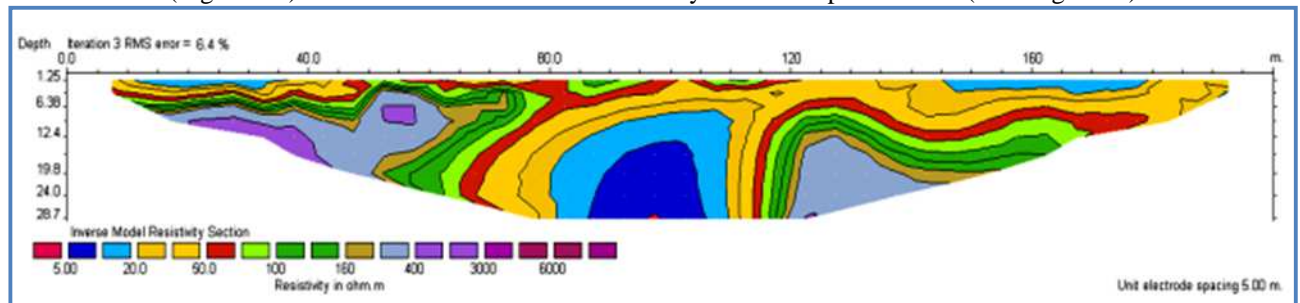


(Figure - E) Inverse model of electrical resistivity section for profile no. 5 (Klebang Putra)
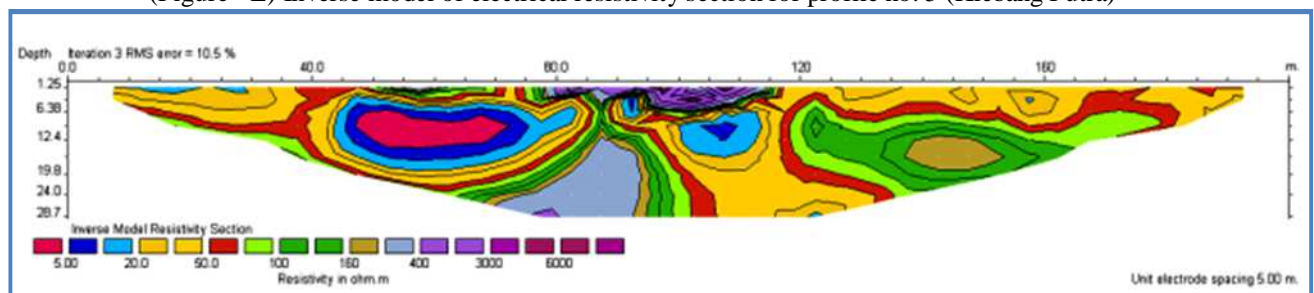


(Figure - F) Inverse model of electrical resistivity section for profile no. 6 (Klebang Putra)

This site is located in the West flank of Kinta valley, situated over a high topographic area and a flat terrain of marbleized limestone rocks, covered with soil. In resistivity Profile #1, the sinkhole appears in the core between electrode 17 and electrode 28, with an unbalanced centre between electrode 21 and 22. It stretches in resistivity Profile #2 under these same aspects. In resistivity Profile #4, the position of this sinkhole differentiates, forming itself between electrode 12 and electrode 23, with an uneven centre between electrodes 19 and 20. In resistivity Profile #6, the position of this sinkhole varies, and also comes into view between electrode 18 and electrode 26, with an uneven centre between electrodes 21 and 22. The depth of this sinkhole varies; in resistivity profile #1, it commences from the shallowest subsurface depth of <3.0m, and continues down to a depth of >28.7m, the bottom being unnoticeable with same aspect mirroring resistivity profiles #2, #3, #4, #5 and #6.

This sinkhole comprises of sediments, with several categories of resistivity values with wide differences, ranging between<5Ω-m and 160 Ω-m. In resistivity profiles #1 and #2, the range differs between 20 Ω-m and160Ω-m, while in resistivity profiles #3 and #4, the range differs between 50 Ω-m -160Ω-m. Finally, in resistivity profiles #5 and #6, the variation in the range lies between <5Ω-m - 160 Ω-m.

The ideal representation of sediments section placed in this sinkhole originated from resistivity profile#5, with resistivity values in the range between 5Ω-m and 160 Ω-m. The section appears from the upper subsurface downward are as follows:

- Top deposits, low mineralized clay with low resistivity.
- From then on, sandy or silty clay with average resistivity.
- Subsequently, silty sand with average resistivity.
- Afterward, sand with above average resistivity.
- Beneath this, transitional zone consisting of limestone rock fragments and sand with high resistivities.
- In the middle of this sinkhole, several categories of resistivity values appear as follows:
- Soft clay with ponged water, highly mineralized, extremely low resistivity's and very high electrical conductivity opening in the middle of sinkholes from a depth of 14.0m.to attain a depth of >28.0m.

- Moderate mineralized clay with very low resistivity's and elevated electrical conductivity adjacent the upper irregularity from a depth of 6.38m, to reach a depth of >28.0m.

This suggests that the origin of this sinkhole might be from pre-existing fractures, which probably widened due to subsidence movement in the area, causing the top layers to crumble down onto the limestone bedrock. This is then swiftly filled with clay and other materials due to the activity of run-off water on its face. In resistivity profile #1, patterns of lower resistivity representing oval – shaped lens are experimental between electrode 30 to electrode 36 in the shallowest subsurface from a depth of <2.25m, onwards to a depth of ~ 12.4m. This lens contains deposits with resistivity's values in the series of 5Ω-m-50Ω-m. Ambiguity with patterns of lower resistivity representing depression with tubular – shapes were detected in resistivity profile #3, at the subsurface directly to the right flank between electrode 23 and electrode 30, and from a depth of ~1.25 m, enduring down to a depth of <6.38m. This depression bears several types of resistivity values in the range of 10 Ω-m - 70 Ω-m. This abnormality mostly consisted of organic grey clay, which is deposited from the old swamp, partially extended into resistivity profile #2, and visibly into resistivity profile #4 and profile #5. A supplementary anomaly, similar to that described above, was detected in resistivity Profile #5; containing several categories of resistivity values in the range of 10 Ω-m - 70 Ω-m, at the shallowest subsurface directly at the left flank between electrode 3 and electrode 8, commencing from a depth of ~1.25m, and continuing down to a depth of < 3.0m.

Most of the sediments that are deposited in resistivity profile #6 form oval - shaped lenses, consisting of diverse patterns of resistivity values, one of which was shown in the subsurface directly at the left flank between electrode 10 and electrode 18, from a depth of 1.25m down to a depth of 23.0m, also containing several categories of resistivity values in the range of>5Ω-m - 50Ω-m, and appearing from the core, extending outwards as follows**:**

- Vastly mineralized soft clay with ponded water, extremely low resistivities, representing the core of the lens.
- Moderately mineralized clay with very low resistivites adjoining the core.
- Low mineralized clay with low resistivities in the external most layers of the lens.

The uppermost of the subsurface layer in resistivity profile #6 were of higher resistivity, representing boulders of weathered limestone, and/or fragments of limestone or other rocks, gravel amalgamated with friable sand, emerging between electrode 11 and 14, then between electrode 17 and 24, from a depth of 1.25 m deep, to a depth of ~ 7.0 m.

A cavity appeared in the sand at the right flank of resistivity profile #6, between electrode 25 and electrode 34, from a depth of ~ 11.0m to~15.0m, typically filled with remaining sediment and rock fragments. All of the Karst features that are detected through the survey in construction site#1 were described in Table 4.

**Table 3: Describes the range of resistivity values with the expected geological unit's deposit.**

| DATA BASE OF KARST FEATURES FROM 2-D ELECTRICAL RESISTIVITY IMAGES SECTIONS IN CONSTRUCTION SITE#1( PUTRA KLEBANG) | | | | | | |
|---|---|---|---|---|---|---|
| **Traverses No.** | **Karst Features** | **Quantity** | **Location** | **Size** | **Approximate Depth** | **Descriptions** |
| Trav.#1 | Sinkhole<br><br>Lens | 1<br><br>1 | E17-E28<br><br>E30-E36 | Diameter~55.0m<br><br>Width 30.0m | 1.25m->28.7m<br><br>>2.25m-12.4m | Subsidence sinkhole, in-fill with stiff, non stiff clay, silty and sand.<br>Oval shape lens in-fill with non stiff clay and ponded water. |
| Trav.#2 | Sinkhole | 1 | E15-E28 | Diameter ~65.0m | 1.25m - 28.7m | Subsidence sinkhole in-fill with stiff clay, non stiff, silty and sand. |
| Trav.#3 | Sinkhole<br><br>Small Depress | 1<br><br>1 | E10-E27<br><br>E23-E30 | Diameter ~85.0m<br><br>Length~35.0m | 1.25m -24.0m<br><br>1.5m-9.0m | Subsidence sinkhole in-fill with stiff clay, non stiff, silty and sand.<br>In-fill with non stiff and stiff clay. |
| Trav.#4 | Sinkhole<br><br>Small Depress | 1<br><br>1 | E12-E23<br><br>E24-E31 | Diameter ~55.0m<br><br>Length~35.0m | 1.25m -24.0m<br><br>1.5m-11.0m | Subsidence sinkhole in-fill with stiff clay, non stiff, silty and sand.<br>In-fill with stiff and non stiff clay with ponded water. |
| Trav.#5 | Sinkhole<br><br>Small Depress | 1<br><br>1 | E16-E26<br><br>E27-E34 | width ~50.0m<br><br>Length ~35.0m | 1.25m ->28.7m<br><br>0.0m-12.4m | Subsidence sinkhole in-fill with stiff clay, non stiff, silty and sand.<br>In-fill with stiff and non stiff clay with ponded water. |
| Trav.#6 | Sinkhole<br><br>Lens<br><br>Lens<br><br>Cavity<br><br>Depression | 1<br><br>1<br><br>1<br><br>1<br><br>1 | E18-E26<br><br>E10-E18<br><br>E24-E27<br><br>E25-E34<br><br>E26-E35 | Diamerter~35.0<br><br>width~40.0m<br>width~15.0m<br>width~45.0m<br>Length~45.0m | 1.25m ->28.7m<br><br>1.25m -23.0m<br><br>~4.50m-18.0m<br><br>11.0m-15.0m<br><br>0.0m-9.0m | Subsidence sinkhole in-fill with stiff clay, non stiff, silty and sand.<br><br>Oval shape, packed with non stiff clay and ponded water.<br>Oval shape, packed with non stiff clay and ponded water.<br>Packed with rock fragments.<br><br>In-fill with stiff clay. |

**Table 4: Data base of karst features from 2-D electrical resistivity images sections in construction site#1**

| No. | Range of resistivity values | Expected geological units deposits | Color of Res. units in ERT model |
|---|---|---|---|
| 1. | 0 Ω-m – 5 Ω-m | Insufficient low resistivity, Soft clay with water filled porosity, very high mineralized. | |
| 2. | 5 Ω-m – 10 Ω-m | Extremely low resistivity and very high conductivity, soft clay with ponded water, highly mineralized. | |
| 3. | 10 Ω-m – 20 Ω-m | Very low resistivity and very high conductivity, Clay moderate mineralized. | |
| 4. | 20 Ω-m – 50 Ω-m | Clay low mineralized, low resistivity and very high conductivity. | |
| 5. | 50 Ω-m – 70 Ω-m | Below average resistivity, soil, silty or sandy clay. | |
| 6. | 70 Ω-m – 100 Ω-m | Average resistivity, clayey or silty sand. | |
| 7. | 100 Ω-m – 160 Ω-m | Above average resistivity, sand friable, coarse grain. | |
| 8. | 160 Ω-m – 200 Ω-m | Mostly high resistivity, transitional zone consists of rock fragments and sand. | |
| 9. | >200 Ω-m – 400 Ω-m | high resistivity, weathered limestone, probably consisting of wet joints or fractures and/or clay in-fill, higher resistivity | |
| 10. | >400 Ω-m – >3000 Ω-m | Very high resistivity, Compact or intact limestone. | |
| 11. | >3000 Ω-m – 6000 Ω-m | Extremely high resistivity, Voids or cavity, air in-fill. | |
| 12. | >4000 Ω-m – 8000 Ω-m | Extraordinarily high resistivity, Intact pure marbleized limestone or dolostone rocks. | |

Figure (13-A, B, C, D, E, F) clearly shows the jointed limestone bedrocks, which are probably made of wet fractured and/or water or clay in-fill, positioned underneath and adjoined to the sinkhole. The surface of this bed was irregular, and contains topography with uplifting and hollow space or pits. This unit indicated the remaining unique limestone formation appearing after a procedure of dissolving into subsurface karsts. The intensity of this bed varies between ~6.5m - ~12.0 m in the left flanks, and tumbling down in the middle of these profiles to get a depth of> 28.8 m, reappearing at the right flank at a depth of ~9.0 - ~19.0m. Uninterrupted bedrock of undamaged or un-weathered limestone of very high resistivity was found at this site, beneath and adjoining the jointed limestone observed in the left flank at a depth of ~8.0 m - ~15.0 m, continuing deep in order to reach a depth of>28.0 m at the core of these profiles. It reappears at the right flank, at a depth of ~24.0m - ~26.0 m. Quite a few pinnacles were observed in the subsurface of this site between a depth of ~6.0 m - ~19.0 m; Figure (13- A, B, C, D, E, F). The intensity of weathered, un-weathered or intact limestone bedrock and the depth of pinnacles in construction site#1 were viewed in Table 7.

**8.2 The interpretation of resistivity profiles in Construction site #2**

The electrical resistivity data gathered in this construction site was calculated in the dearth of borehole control by utilizing Table 3. This site is located to the east flank of Kinta valley, and is normally over a high topographical area and a flat terrain of marbleized limestone rocks. The top of the subsurface is categorized by high resistivity; interpreted as a zone of near surface weathered limestone and/or highly jointed limestone, with boulders of solid limestone and rock fragments.

**Figure 14: Inverse model of electrical resistivity section form profiles#1 to profiles#6, viewing the interpreted location of shallow karst features (sinkholes and cavities) in Construction site #2 (Klebang Restu)**
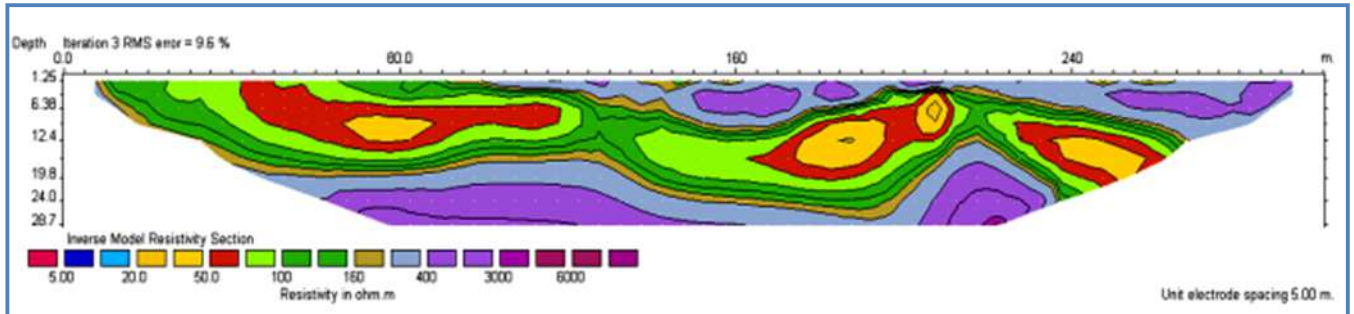


(Figure - A) Inverse model of electrical resistivity section for profile no. 1 (Klebang Restu)
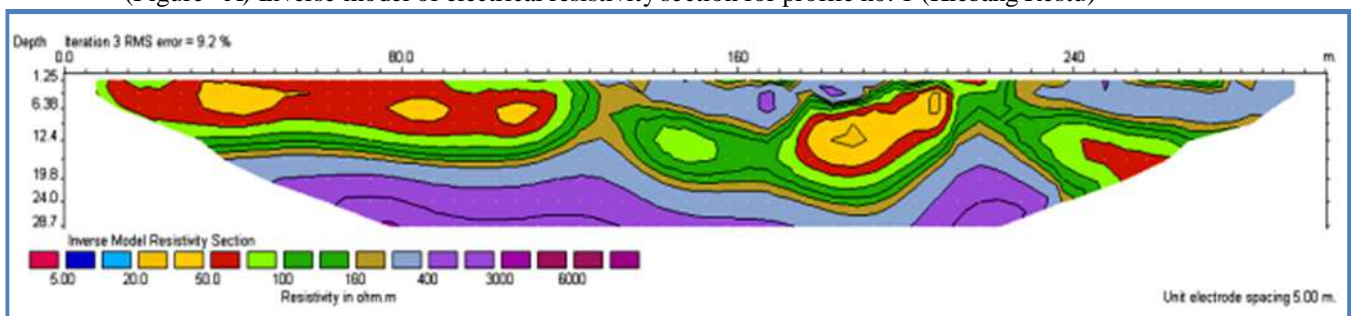


(Figure - B) Inverse model of electrical resistivity section for profile no. 2 (Klebang Restu)
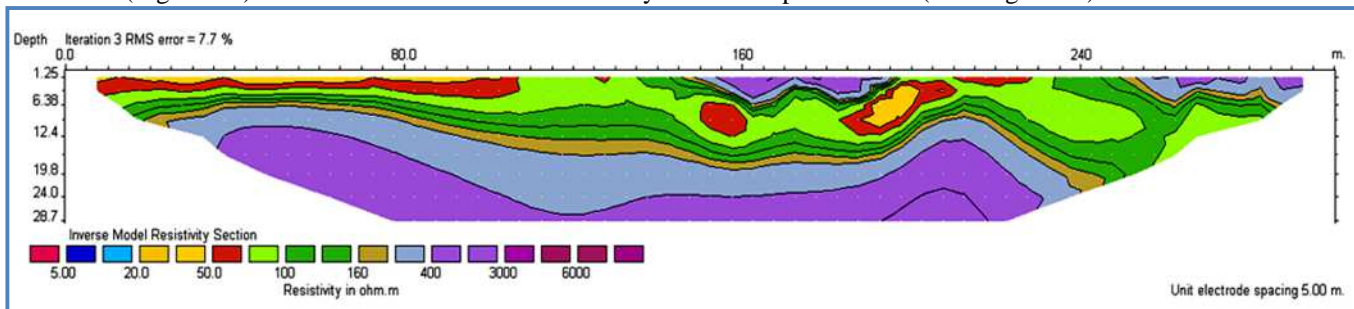


(Figure - C) Inverse model of electrical resistivity section for profile no. 3 (Klebang Restu)
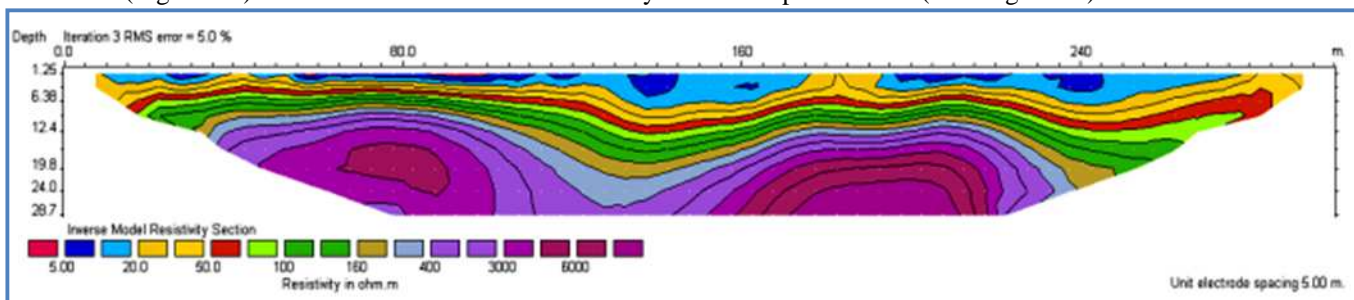


(Figure - D) Inverse model of electrical resistivity section for profile no. 4 (Klebang Restu)
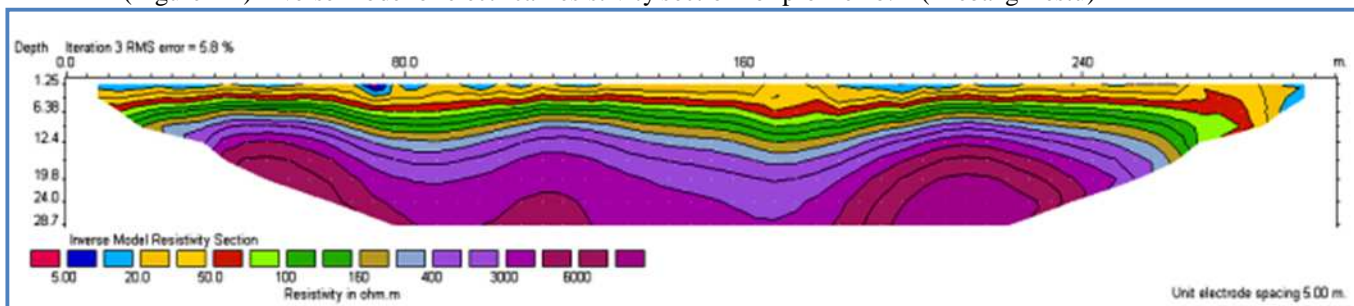
(Figure - E) Inverse model of electrical resistivity section for profile no. 5 (Klebang Restu)
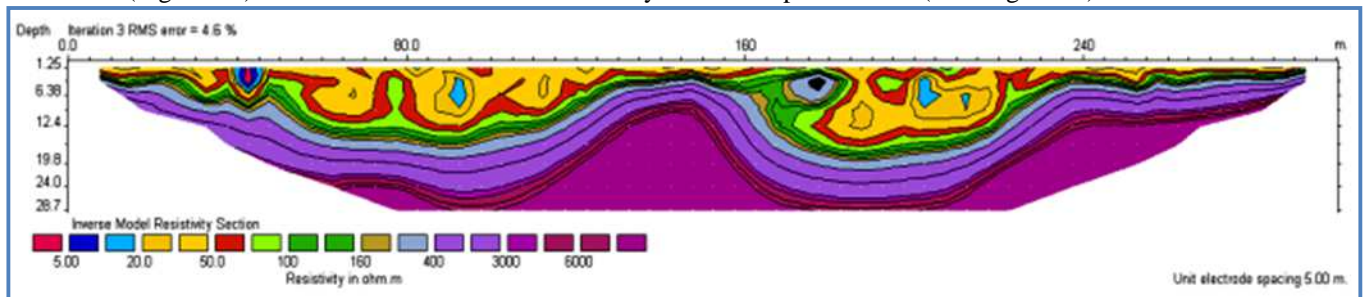


(Figure - F) Inverse model of electrical resistivity section for profile no. 6 (Klebang Restu)

The interpretation confirms that a zone of irregular sub-surface magnitudes in this site is extended between resistivity Profile #1 and Profile #3 in the shape of one longitudinal asymmetrical tubular channel. Sinkholes were detected near the surface in resistivity profile #2, commencing in the shallowest subsurface between electrode 40 and electrode 58 in the right flank, from a depth of <1.25m, sustaining deep in order to reach a depth of ~24.0 m. It appears as a slim to medium wide throat, extending to about 40 m in diameter. The centre of the sinkhole appears in this profile, and expanded in profile#1 and profile#3. This sinkhole was linked to one or asymmetrical tubular channel along these profiles. Tubular cavities of visually undetermined depth emerged as oval-shaped lenses, merging together into one tubular channel; Figure (14-A, B, C).

The abnormality detected in resistivity profile #1, profile#2 and profile #3 commenced approximately from electrode 3 to electrode 55 in profile #1, and to electrode 58 in profile #2, and in profile #3, originated in the shallowest subsurface from a depth of <1.25m, and are sustained deep into the right flank in order to reach a depth of ~24.0m. It consisted of deposits with several categories of resistivity values in the range of 20 Ω-m to 160 Ω-m, and extends outwards from internal to the external, as follows:

- Low mineralized clay with low resistivity and high conductivity coming out as lenses in this tubular incongruity.
- Sandy or silty clay with below standard resistivity surrounding the deposits before.
- Silty sand with standard resistivity representing the key deposits.
- Sand with above standard resistivity.
- Rock part of limestone and sand with high resistivities.

This implies that the base of all these cavities were from a pre-existing features of joints in the limestone bedrock that was probably created into prominent solution-widened joints, due to the activity of heavy rain and running water on the face, which were then rapidly packed with clay and other materials.

The region of weathered limestone or highly jointed limestone bedrocks extending across these three profiles was seen to be beneath and closest to this longitudinal tubular irregularity, with an overall rough surface, and categorized with higher resistivities. It occurs on the subsurface at a depth of 6.36m - ~9.0m, and moved downwards to reach a depth of ~12.0m - ~17.0 m at the core of this profile, then dropped down to reach a depth of~17.0m -26m. After that, it again rises up to reach a depth of~7.0m-12.0m in the right flank; Figure (14-A, B, C).

Undamaged or non-weathered limestone bedrocks with very high resistivity were discovered in the subsurface at a depth of ~19.8m along the left flank, in profile #1, profile#2 and profile#3. It tumbled down to achieve a depth of >27.0 m in the core, and continued to the right flank, arising up in the shape of a crest in order to reach a depth of ~12.4m Figure; (14-A, B, C). Numerous pinnacles of limestone were observed in the subsurface in profile #1, profile #2 and profile#3, which were at a depth of ~11.5 m - ~12.4 m, Figure; (14-A, B, C). In Resistivity Profile#4 and Profile #5, the cover karst deposits expanded from electrode 3 to electrode 58. Two depressions were observed in the resistivity section, one of which was between electrodes 10-36, while the other between electrodes 40-56. The utmost depth of these depressions was between ~11.5m -~13.0m for the one at the centre of this profile, and a depth of ~13.5m for the one in the right flank of this profile, Figure (14-E).

A number of categories of resistivity values in the range of 20Ω-m to 160 Ω-m emerged with these deposits. Limestone bedrock with karstification features was clearly detected in the subsurface of both flanks, with twin centres appearing beneath electrode 29 and electrode 49 in resistivity Profile#4. It comes with a tri-centre in resistivity Profile#5. This irregular zone of weathered limestone expanded across this profile beneath the upper layers, which was overall characterized by higher resistivity; starting in the subsurface at a depth of ~6.36m, to make a maximum depth of ~15.5m. Also, in these profiles, intact or unweathered limestone bedrock was found at a depth of ~7.5m to ~12.0m in the left flank, plunging down at a depth of ~9.0m - ~22.0m in the centre, and

at a depth of ~ 17.0 m to - 24.0m in the right flank. Several pinnacles of limestone were discovered in the subsurface beneath these profiles at a depth between ~ 6.0m - ~7.0 m; Figure (14-D, E).

In resistivity profile #6, two depressions were observed in the resistivity section; one between electrode 3 and electrode 29, with a maximum depth of ~15.5m beneath electrode 19, while the other depression was between electrode 30 and electrode 57, with a maximum depth of ~18 m beneath electrode 39. Additionally, deposits with numerous categories of resistivity values are crammed with these depressions, ranging from 20Ω-m to 160 Ω -m, and lenses of lower resistivity values from 10Ω-m to 20 Ω -m were found in the middle of these depressions. Moreover, immature cavities were located in the sand, between electrodes 35 and electrode 37 at a depth of ~1.25m, down to a depth of ~8.0m, ~10m wide, and ~6.75m height, with enormously high resistivity that are typically air-infilled.

Immediately before electrode 9 till electrode 10, a minute sinkhole was observed from the surface down to a depth of ~8.0m, containing several categories of resistivity values ranging from 5Ω-m to 20Ω-m. This sinkhole water is in-filled, and typically consists of soft clay with ponded water. Sufficiently mineralized clay was found adjacent to the preceding deposit. The existence of clay deposits observed in this site could compromise the site's reliability, as the clay could fall down or disrupt piping when situated under load, due to the weight of the structures.  All of the Karst features, which were detected through the survey in construction site #2, were described in Table 5.

**Table 5:  Data base of karst features from 2-D electrical resistivity images sections in construction site#2**

| DATA BASE OF KARST FEATURES FROM 2-D ELECTRICAL RESISTIVITY IMAGES SECTIONS IN CONSTRUCTION SITE#2 ( KLEBANG RESTU) | | | | | | |
|---|---|---|---|---|---|---|
| Traverses No. | Karst Features | Quantity | Location | Size | Approximate Depth | Descriptions |
| Trav.#1 | Large longitudinal asymmetrical tabular channel | 1 | E3-E58 | Length 260.0m | 9.25m-28.7m | In-fill with stiff clay ,silty sand and sand |
| Trav.#2 | Sinkhole | 1 | E40-E58 | Diameter ~40.0m | <1.25m - 24.0m | Rain water dissolution activity |
| | Large longitudinal asymmetrical tabular channel | 1 | E3-E58 | Length ~260m | 9.25m-28.7m | In-fill with stiff clay ,silty sand and sand |
| Trav.#3 | Sinkhole | 1 | E40-E58 | Diameter~40.0m | <1.25m - 24.0m | Rain water dissolution activity |
| | Large longitudinal asymmetrical tabular channel | 1 | E3-E55 | Length ~260.0m | 9.25m-28.7m | In-fill with stiff clay ,silty sand and sand |
| Trav.#4 | Depression | 1 | E10-E36 | width ~130.0m | 0.0m-17.0m | Due to Karst processes. |
| | Depression | 1 | E40-E56 | width~130.0m | 0.0m-17.0m | Due to Karst processes. |
| Trav.#5 | Depression | 1 | E11-E23 | Length ~60.0m | 0.0m-9.50m | Due to Karst processes. |
| | Depression | 1 | E26-E43 | Length ~160.0m | 0.0m-11.50m | Due to Karst processes. |
| Trav.#6 | Depression | 1 | E3-E29 | Length ~120.0m | ~15.5m | in-fill with stiff and non-stiff clay |
| | Depression | 1 | E30-E57 | Length ~105.0m | ~18.0m | in-fill with stiff and non-stiff clay |
| | Immature cavity | 1 | E35-E37 | Size10.0X6.75m | 1.25m-8.0m | air in-fill |
| | Minute sinkhole | 1 | E9-E10 | Diameter ~5.0m | 0.0m -8.0 m | in-fill with water and non -stiff clay |

The limestone bedrock that was visibly observed in the subsurface along this profiles possesses very high resistivities, with the development of karstification phenomena, which describes rough carbonate bedrock

containing many peaks and troughs, starting with a zone of weathered limestone, and/or highly widened jointed limestone bedrock expanding across this profile, overlooking the upper layers at a depth of ~3.5m down in order to reach a maximum depth of ~18.0m that was overall characterized by higher resistivity. This was maintained by intact or unweathered limestone bedrock with very high resistivity, observed on the subsurface at a depth of ~4.0m on both flanks, tumbling down to reach a maximum depth of ~22.0m in the centre.

Limestone pinnacles were noticeably observed at the subsurface in the middle of this resistivity profile, between depths of ~3.5m to ~4.0m Figure (14-F). The depth of weathered, unweathered or integral limestone bedrocks and pinnacles in construction site#2 was presented in Table 7.

### 8.3 The interpretation of resistivity profiles in Construction site #3

This site is normally situated over a high topography area and a flat terrain of marbleized limestone rocks. The electrical resistivity data accumulated in this construction site was clarified in the deficiency of borehole control, by utilizing data posited in Table 3. The interpretation confirms that a variety of sinkholes that are present in this site, mainly the soil cover collapse type and unmitigated, can clearly be seen between resistivity Profile #3 and Profile #6, Figure -15.

**Figure 15: Inverse model of electrical resistivity section form profiles#1 to profiles#6, viewing the interpreted location of shallow karst features (sinkholes and cavities) in Construction site #3 (Bandar Baru Putra)**
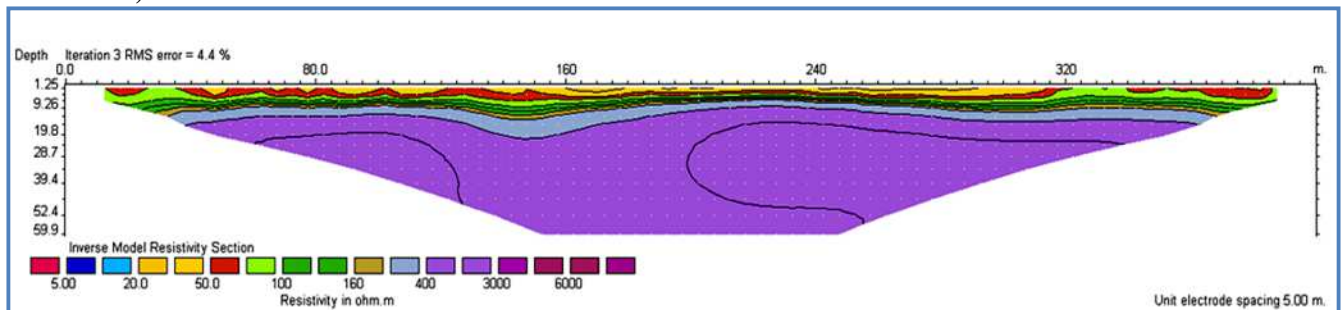


(Figure - A) Inverse model of electrical resistivity section for profile no. 1 (Bandar Baru Putra)
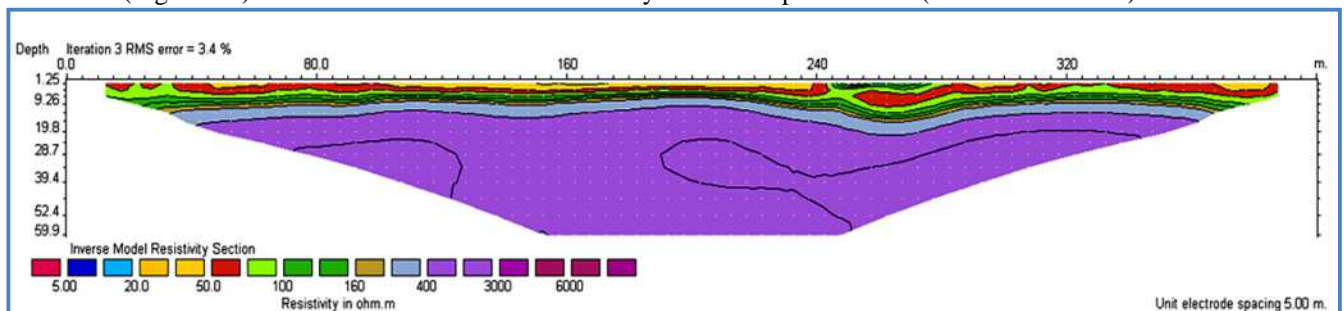


(Figure - B) Inverse model of electrical resistivity section for profile no. 2 (Bandar Baru Putra)
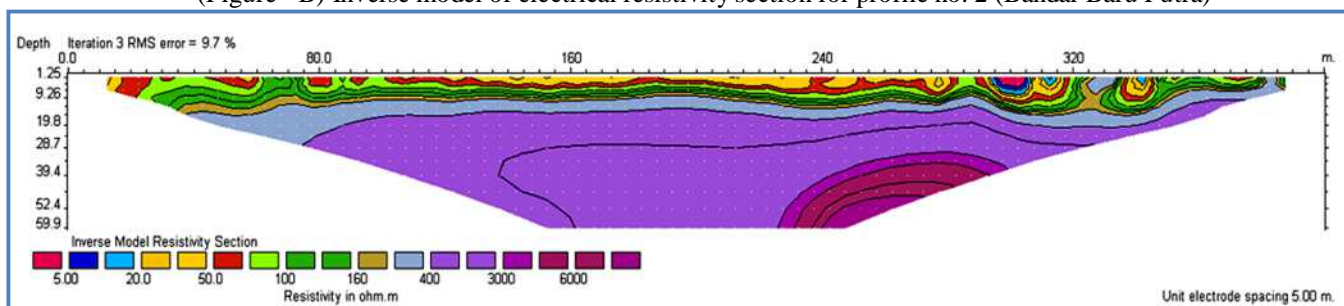


(Figure - C) Inverse model of electrical resistivity section for profile no. 3 (Bandar Baru Putra)
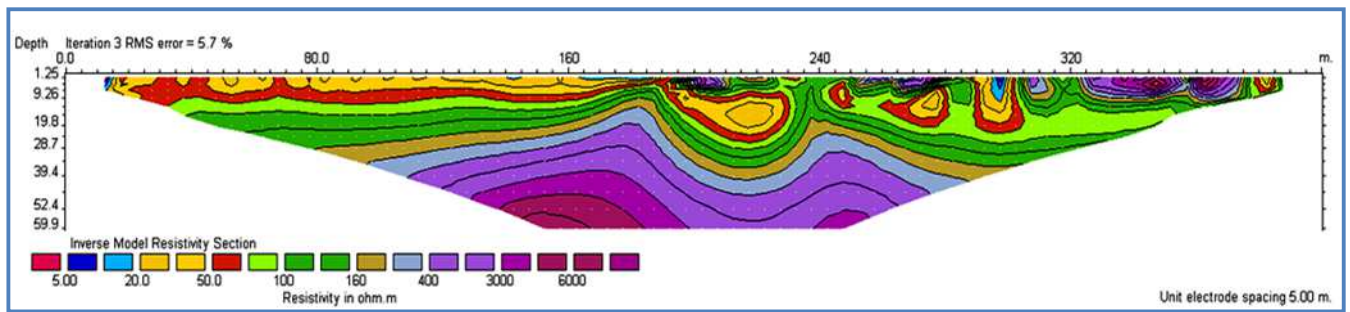
(Figure - D) Inverse model of electrical resistivity section for profile no. 4 (Bandar Baru Putra)
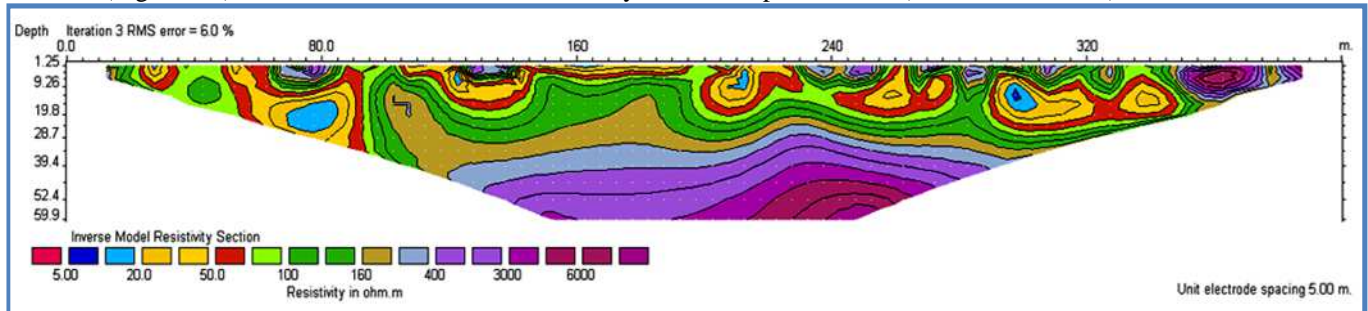


(Figure - E) Inverse model of electrical resistivity section for profile no. 5 (Bandar Baru Putra)
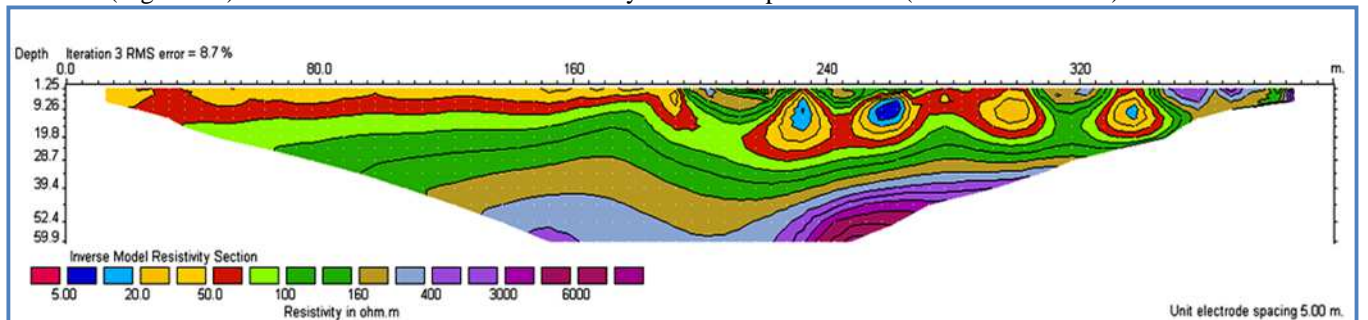


(Figure - F) Inverse model of electrical resistivity section for profile no. 6 (Bandar Baru Putra)

Zones with semi-regular surface and subsurface magnitudes are found along two traverses; traverse#1 and traverse #2. Adjacent to the middle of resistivity traverse #1 for the left flank, small depression began in the shallowest subsurface beneath and almost between electrodes 25 and electrode 38, with a depth of ~15.00m; Figure (15 - A). Close to the middle of resistivity traverse #2 from the right flank, small depression began in the shallowest subsurface beneath and near electrodes 49 and electrode 61, with a depth of ~15.0m; Figure (15 - B), while in traverse #3, the subsurface limestone becomes irregular, and small depression began in the shallowest subsurface beneath and between electrodes 3 and electrode 27, with a depth of ~16.00m, with the other beneath and between electrodes 49 and 65, having a depth of ~16.0m. Many small size sinkholes along this traverse appears mostly in the right flank as the soil cover collapse type, merging into the sand, some with water in its core, having a depth of ~16.00m; Figure (15 - C). Limestone bedrocks, with very high resistivity were found in the subsurface between a depth of ~4.0m to 9.26m along profile #1, profile #2 and profile #3. It tumbled down to achieve a depth of >17.0m; Figure (15 -A, B, C).

Abnormalities were detected in resistivity traverse #4, traverse #5 and traverse #6. In the case of traverse #4, a sinkhole appears between two pinnacles in middle of this traverse, commencing approximately from electrode 38 to electrode 47 in the shallowest subsurface, from a depth of 3.25m, and sustained deep into the right flank in order to reach a depth of ~37.0m. It consists of deposits with several categories of resistivity values in the range between 20 $\Omega$-m and 160 $\Omega$-m and extends outwards from internal to the external as follows:

- Low mineralized clay with low resistivites and high conductivity in the core, coming out as lenses in these oval –shaped sinkholes.
- Sandy or silty clay with below standard resistivites, surrounding the deposits before.
- Silty sand with standard resistivites, representing the key deposits.
- Sand surpassing standard resistivites.
- Rock fragments of limestone and sand, with high resistivities surrounding the sinkhole.

This type of sinkhole appears due to the activity of the karst processes. Several soil cover collapse sinkholes

appear in the right flank, with maximum depth of ~19.8m.

The presence of water in this type of sinkhole are indicative of the origin of heavy rain running off on the face of the surface, which were then rapidly packed with clay and other materials in these pipes, Figure (15 -D). Sections of weathered limestone or highly jointed limestone bedrocks extending across profiles#3 and profile#4 was seen beneath, with an overall uneven surface containing several pinnacles, and categorized with higher resistivity. The pinnacles have a depth between 9.26m -19.5m. In Resistivity profile #5, the subsurface karst deposits expanded from electrode 4 to electrode 78. The utmost depth of these deposits was between ~37.50m in the left flank of this profile, to less near the middle, reaching a depth of 19.8m in the left flank, with a depth of ~34.5m; Figure (15-E). A number of categories of resistivity values in the range of 20 Ω-m to 160 Ω-m were observed in the resistivity image section. Numerous types of karst features were observed in this profile emerging within the deposits, with its presence in the shape of the soil pipes, multi lenses, and empty sinkholes.

Limestone bedrock with karstification phenomena was visibly observed in the subsurface at the centre, appearing beneath electrode 26 and electrode 62 in resistivity profile #5. This irregular zone of weathered limestone expanded across this traverse beneath the upper layers, which was overall characterized by higher resistivities. The opening in the subsurface at a depth a maximum depth of ~39.5m in the left flank, rises up to reach a depth of ~22.0m in the middle, which then dropped to reach a depth of 37.0m in right flank of this profile. Rock head pinnacle of limestone was also discovered in the subsurface; Figure (15 - E).

In resistivity profile #6, the resistivity section showed massive depression extended along this profile beneath electrode 3 and electrode 78, containing deposits with various categories of resistivity values ranging from 20Ω-m to 160 Ω -m. Multi-lenses of lower resistivity values from 10 Ω-m to 20 Ω -m were found to be extended between electrode 46 and electrode 61, with a depth reaching ~22.0m. Additionally, mature sinkholes were located between electrodes 66 and electrode 69, from the surface down to a depth of ~19.8m, and a width of ~15.0m, containing several categories of resistivity values ranging from 5 Ω-m to 70 Ω -m. These sinkholes are typically in-filled with rainwater, and also consist of soft clay with pond water; Figure (15 - F).

Stiff clay was found adjacent to the preceding karstic deposit within the depression observed existence between electrode 7 and electrode 42 at this site, and could compromise the reliability of this site, as clay could fall down by itself, or on piping when situated under load, due to the weight of the structures. All of the Karst features, which were detected through the survey in construction site#3, were described in Table 6.

**Table 6:  Data base of karst features from 2-D electrical resistivity images sections in construction site#3**

| Traverses No. | Karst Features | Quantity | Location | Size | Approximate Depth | Descriptions |
|---|---|---|---|---|---|---|
| DATA BASE OF KARST FEATURES FROM 2-D ELECTRICAL RESISTIVITY IMAGES SECTIONS IN SITE#3 (NORTH BANDER BARU PUTRA) | | | | | | |

| Traverses No. | Karst Features | Quantity | Location | Size | Approximate Depth | Descriptions |
|---|---|---|---|---|---|---|
| Trav.#1 | Depression | 1 | E25-E38 | Length ~65.0m | 7.5m-15.0m | In-fill with stiff and silty clay. |
| Trav.#2 | Depression | 1 | E49-E64 | Length ~75.0m | 7.5m-15.0m | In-fill with stiff and silty clay. |
| Trav.#3 | Depression | 1 | E3-E27 | Length ~120 m | 3.5m-16.0m | Rain water activity. |
|  | Depression | 1 | E49-E65 | Length ~80.0m | 3.0m-16.0m | Rain water activity. |
|  | Sinkhole | 1 | E61-E65 | Diameter ~20.0m | 0.0m-17.5m | Soil covers collapse. |
|  | Sinkhole | 1 | E68-E70 | Diameter ~10.0m | 0.0m-16.0m | Soil covers collapse. |
| Trav.#4 | Sinkhole | 1 | E38-E47 | Diameter ~45.0m | 3.25m-37.0m | Karst processes. |
|  | Soil pipe | 1 | E50-E51 | Diameter ~5.0m | 0.0m-15.0m | Soil covers collapse. |
|  | Soil pipe | 1 | E57-E58 | Diameter ~5.0m | 0.0m-17.0m | Soil covers collapse. |
|  | Soil pipe | 1 | E59-E61 | Diameter ~10.0m | 0.0m-19.8m | Soil covers collapse. |
|  | Soil pipe | 1 | E77-E78 | Diameter ~5.0m | 0.0m-7.50m | Soil covers collapse |
| Trav.#5 | Soil pipes | 1 | E06-E08 | Diameter ~10.0m | 0.0m - 9.7m | Soil covers collapse. |
|  | filled depress | 1 | E14-E18 |  | 0.0m -19.0m | Sand in-fill |
|  | Soil pipes | 1 | E53-E54 | Diameter ~20.0m | 0.0m -19.0m | Soil covers collapse. |
|  | Multi lenses | 1 | E59-E70 | Diameter ~5.0m | 9.0m -19.0m | Stiff & non-stiff clay. |
|  | Empty depress | 1 | E22-E30 | Width ~55.0m | 0.0m -19.8m | Rain water dissolution. |
|  | full-size lens | 1 | E11-E19 | Diameter ~40.0m Width ~80.0m | 9.25m-28.7m | Stiff clay with ponded water. |
| rav.#6 | Sinkhole | 1 | E66-E69 | Diameter ~15.0m | ~19.8m | in-fill with rain water |
|  | Multi lenses | 3 | E46-E61 | Width ~75.0m | ~22.0m | clay with ponded water |
|  | Depression | 1 | E7-E42 | length~210.0m | 19.0m | in-fill with non-stiff clay |

The uneven marbleized limestone bedrock was visibly observed in the image extended on the subsurface between electrodes 28 to electrode, from a depth of 29.0m, to maximum depth of > 52.4m. It began with a zone of weathered limestone and/or highly widened jointed marbleized limestone bedrock, overlooking upper layers deposits. Intact or unweathered limestone bedrock, with very high resistivities were observed on the subsurface beneath the weathered bedrock, tumbling down to reach a maximum depth of >59.0m in the left flank of the profile. The depth of weathered, un-weathered or integral limestone bedrocks and pinnacles in construction site#3 was presented in Table 9.

## 9.    Depth of marbleized limestone bed rock in the study construction sites

Nearby karst terrains normally create problems for engineers. Often, only engineers who are familiar with soluble rock understand these anomalies and problems that are associated with it. For engineers, limestone creates various difficulties that are made complex by increased expansion of the karsts morphology.  The three tables below present an outline or portrayal of some selected points regarding the limestone bedrock depth of the three construction sites that will be favourable for engineers for them to recognize the depth of limestone in the three sites under study. These are, however, incomplete, and can only provide common suggestions of projected ground conditions, despite the possibility of ending up with enormous discrepancies regarding the depth of the local feature. The surveys showed that the depth of marbleized limestone bedrock in these three construction sites was uneven, and possesses many pinnacles and cutters.

**Table 7: Described the approximate depth of weathered, intact marbleized limestone bedrock and pinnacles in construction site#1**

| No. | site #11 | Electrode No | Approximate depth of weathered limestone | Electrode No | Approximate depth of intact limestone bedrock | Electrode No | Approximate depth of pinnacle |
|---|---|---|---|---|---|---|---|
| 1. | Res Trav. #1 | 7<br>11<br>16<br>18<br>19 - 24<br>28 | 11.0 m<br>13.0 m<br>8.0 m<br>19.8 m<br>>28.0 m<br>19.0m | 8<br>11<br>15 | 15.0 m<br>18.0 m<br>14.0 m | 16<br>28 | 7.0 m<br>19.0 m |
| 2. | Res Trav. #2 | 5<br>9<br>17<br>18 | 10.0 m<br>12.4 m<br>24.0 m<br>> 28.0 m | 10<br>16<br>17 | 19.0 m<br>24.0 m<br>> 28.0 m | - | - |
| 3. | Res Trav. #3 | 4<br>12<br>16 - 25<br>31 | 6.5 m<br>18.0 m<br>> 28.0 m<br>9.0 m | 4<br>9<br>14 | 10.0 m<br>8.5 m<br>> 28.0 m | 10 | 6.0 m |
| 4. | Res Trav. #4 | 4<br>9<br>13<br>15<br>23<br>33 | 8.5 m<br>6.38 m<br>18.0 m<br>> 28.0 m<br>9.0 m<br>12.0 m | 6 - 10<br>12 | 8.0 m<br>19.8 m | 10 | 6.0 m |
| 5. | Res Trav. #5 | 4<br>10<br>12<br>15<br>26<br>30 | 7.0 m<br>10.0 m<br>3.0 m<br>> 24.0 m<br>12.0 m<br>22.0 m | 5<br>9<br>10<br>15 - 24<br>26 | 8.0 m<br>10.0 m<br>18.0 m<br>> 28.0 m<br>> 26.0 m | 12<br>26 | 3.0 m<br>11.0 m |
| 6. | Res Trav. #6 | 15<br>19<br>20 | 26.0 m<br>12.0 m<br>> 28.0 m | 16 - 17 | 26.0 m | 19 | 12.0 m |

**Table 8: Described the approximate depth of weathered, intact marbleized limestone bedrock and pinnacles in construction site#2**

| No. | site #12 | Electrode No | Approximate depth of weathered limestone | Electrode No | Approximate depth of intact limestone bedrock | Electrode No | Approximate depth of pinnacle |
|---|---|---|---|---|---|---|---|
| 1. | Res Trav. #1 | 21 - 59<br>9 - 26<br>38<br>44 | 1.25 m<br>15.0 m<br>26.0 m<br>11.0 m | 13<br>36<br>44 | 23.0 m<br>> 28. 0 m<br>15.0 m | 43 | 12.4 m |
| 2. | Res Trav. #2 | 27 - 40<br>47 - 57<br>9 - 21<br>26<br>38<br>43 | 1.25 - 16.0 m<br>1.25 - 9.0 m<br>15.0 m<br>12.0 m<br>26.0 m<br>12.0 m | 11 - 21<br>38<br>44 | 19.8 m<br>> 28.0 m<br>17.0 m | 26<br>44 | 12 4 m<br>11.5 m |
| 3. | Res Trav. #3 | 6<br>12<br>33<br>43 | 9.0 m<br>6.38 m<br>17.0 m<br>7.0 m | 8<br>25<br>43 | 19.8 m<br>>27.0 m<br>12.4 m | 11<br>43 | 6.36 m<br>9.5 m |
| 4. | Res Trav. #4 | 6<br>28<br>43 | 9.0 m<br>15.5 m<br>6.36 m | 8<br>28<br>43<br>50 | 12.0 m<br>22.0 m<br>10.0 m<br>24.0 m | 17<br>43 | 6.0 m<br>7.0 m |
| 5. | Res Trav. #5 | 4<br>17<br>33<br>44<br>54 | 8.0 m<br>10.0 m<br>10.0 m<br>6.0 m<br>14.0m | 10<br>24<br>43<br>54 | 7.5 m<br>9.0 m<br>8.5 m<br>17.0 m | 10<br>24<br>44 | 6.0 m<br>6.36 m<br>6.0 m |
| 6. | Res Trav. #6 | 3<br>19<br>30<br>39<br>43<br>59 | 3.5 m<br>18.0 m<br>3.5 m<br>18.0 m<br>3.5 m<br>3.0 m | 3<br>22<br>30<br>39 | 4.0 m<br>18.0 m<br>4.0 m<br>22.0 m | 30<br>49 | 3.5 m<br>4.0 m |

**Table 9: Described the approximate depth of weathered, intact marbleized limestone bedrock and pinnacles in construction site#3**

| No. | site #3 | Electrode No | Approximate depth of weathered limestone | Electrode No | Approximate depth of intact limestone bedrock | Electrode No | Approximate depth of pinnacle |
|---|---|---|---|---|---|---|---|
| 1. | Res Trav. #1 | 17 | 9.26m | 17 | 16.0m | - | - |
|  |  | 33 | 15.0m | 33 | 20.0m | - | - |
|  |  | 49 | 10.0m | 49 | 10.0m | - | - |
|  |  | 65 | 14.0m | 65 | 15.0m | - | - |
| 2. | Res Trav. #2 | 17 | 14.0m | 17 | 17.0m | - | - |
|  |  | 33 | 9.62m | 33 | 18.0m | - | - |
|  |  | 49 | 12.0m | 49 | 18.0m | - | - |
|  |  | 65 | 9.0m | 65 | 15.0m | - | - |
| 3. | Res Trav. #3 | 17 | 16.0m | 17 | 19.8m | - | - |
|  |  | 33 | 15.0m | 33 | 17.0m | - | - |
|  |  | 49 | 17.0m | 49 | 19.8m | - | - |
|  |  | 65 | 16.0m | 65 | 21.0m | - | - |
| 4. | Res Trav. #4 | 17 | - | 17 | - | 37 | 11.0m |
|  |  | 33 | 19.8 | 33 | 27.0m | 49 | 22.0m |
|  |  | 49 | 20.0m | 49 | 27.0m |  |  |
|  |  | 65 | - | 65 | - |  |  |
|  |  |  | - |  | - |  |  |
| 5. | Res Trav. #5 | 17 | - | 17 | - | 46 | 20.0m |
|  |  | 33 | 34.0m | 33 | 42.0m |  |  |
|  |  | 49 | 27.0m | 49 | 29.0m |  |  |
|  |  | 65 | - | 65 | - |  |  |
|  |  |  | - |  | - |  |  |
| 6. | Res Trav. #6 | 17 | - | 17 | - | 33 | 39.4m |
|  |  | 33 | 39.4m | 33 | 52.4m | 56 | 32.0m |
|  |  | 49 | 32.0m | 49 | 42.0m |  |  |
|  |  | 63 | 29.0m | 63 | 34.0m |  |  |

## 10. Results and discussion

The current Electrical Resistivity Tomography (ERT) survey at several divisions of the housing complex structure sites in the north of Ipoh was conducted in order to determine the subsurface geological features, including sinkholes, karstic voids or cavities, and the subsurface geological structures, together with intensely fractured zones and faults. An assessment of the situation was surmised from the subsurface images. Subsequently, an estimation of the possibility of a collapse occurring due to these cavities or voids was prepared.

(1) This study also displayed that high resolution Electrical Resistivity Tomography (ERT) can be effectively implemented to reflect the bedrocks and the fractures in subsurface karsts terrains. The resistivity method used in this study was very favourable vis-à-vis locating underground voids, or cavities and sinkholes, and also water channels, due to the dissolution in fractured zones. It is also completely suitable for differentiating surficial soil, clay, weathered rocks, compact or intact rocks, and air-filled karstic voids or cavities, and intensely fractured rocks. These features effect many construction site locations in areas extended over carbonate rocks, causing disturbance in construction works, which can increase the overall cost of the project(s).

(2) The geological model is clarified via the geophysical data, consisting of a basal limestone unit, which comprises of the bedrock; enclosed by soil or sandy clay. This bedrock unit appears to have been dissected or intervened by cavities that are high-flying to solution-widened joints, and is perceived as the karstic processes. These features are perilous, because they are in-filled with thick clay, while others with sandy or salty clay, which could collapse when subjected to piping under load.

(3) The geophysical data indicated that the depth of limestone bedrock was asymmetrical or uneven, containing many pinnacles and cutters. In construction site #1, the depth of weathered limestone bedrock was mixed between 3.0 m and >28.0m. For intact limestone bedrock, the depth varied between 8.0 m and >28.0m, and the depth of pinnacles varied between 3.0 m and 19.0m, as shown in Table 7. In

construction site #2, the depth of weathered limestone bedrock mottled between 1.25 m and 26.0m. The depth of an intact limestone bedrock varied between 4.0 m and >28.0m, while the depth of its pinnacles varied between 3.5 m and 12.4m, as shown in the Table 8. In construction site #3, the depth of weathered limestone bedrock mottled between 9.00 m and 39.0 m. The depth of intact limestone bedrock varied between 10.0 m and50.0m, and the depth of pinnacles varied between 11.0 m and 39.0 m, as shown in Table 9.

(4) The geophysical data in construction site #1 is indicative of an area of lesser resistivity and high conductive ambiguities, where the top layers had been lowered by fracture along the site and the resulting sinkhole due to the collapse, thus containing soft clay with vast mineralization with some pond water has made the area less resistive to electrical currents. This was noticed on the site during dugout works. The data also exposed that this sinkhole continues to be produced in the subsurface at most of this site, and was in fact extended in six locations of the six resistivity profiles at this site.

(5) The geophysical data in construction site #2 showed an area of lower resistivity and high conductive ambiguities, which has been affected by sinkhole and many tubular ambiguities containing clay and sandy clay. The bedrock unit appears to be littered by many features such as sinkholes, cavities and channels. These features are harmful as they are packed with thick clay, sandy or silty clay, which could collapse when subjected to piping under load. The high resistivity ambiguities are indicative of the existence of karstic voids, which require confirmation via drilling results.

(6) The geophysical data in construction site #3 showed an area that has been affected by several karst features in shape soil cover collapse sinkholes and soil pipes, thus containing clay and sandy clay, and are sometimes in–filled with rain water. These features are harmful as they are packed with clay, sandy or silty clay, which could collapse when subjected to piping under load.

(7) These analyses led to the conclusion that the origin of the sinkhole and cavities in construction site #1 was a pre-existing fracture that had widened, possibly due to subsiding movement in the area, causing the collapse of top layers onto limestone bedrock, which was then rapidly crammed with clay due to the activity of run-off water on the surface. However, the origin of the sinkholes and cavities in construction site #2 appears to be new. The origins of all these cavities were previously thought to be of pre-existing features, such as joints in limestone bedrock. It had formed into a strongly outstanding solution-widened joint for rainfall activity and running off of water on the surface, which was swiftly being packed with clay and other materials.

The origin of the sinkholes and lenses in construction site #3 appears to be a new. The early stages of a soil-cover karst collapse may appear as a soil-piping feature; most soil cover collapse sinkholes locations are soil materials subjugated by porous layers, residual silty-clay soils with bedrock structure of ≥ 9m thickness, highly weathered condition of underlying carbonate bedrock, with positions adjacent to an active sinkhole. The sinkholes in the study area were characterized by referring to the mechanisms of the ground malfunction, and the nature of the material, which fails and subsides. In construction site#1, the sinkhole is a collapse, which a type is created by a small-scale collapse that provided the surface with subsurface structural features. Then, the earliest collapse sinkhole was packed with soil, sediment and fragments due to the modifications to the surroundings, and finally resulting in the sinkhole being buried. Surface subsidence may then take place, due to compaction of the soil.

(8) The sinkhole in construction site#2 is a type of suspension sinkhole, created by the slow dissolution of the limestone bedrock. They are common features, such as joints of a karst terrain developing over geological time scales. The larger features still have potentially unsound rock mass somewhere beneath their lowest point, and the majority dissolution features are deep holes and pipes. These are produced at isolated stream sinks and swallow holes, where the form resembles conical sinkholes, largely created by scattered water percolation.

The sinkhole in construction site#3 is due to the sudden appearance of a soil cover collapse sinkhole, initiated when the development of small voids at a depth of a few meters in soil, or unconsolidated cover overlying karstic bedrock are enlarged by the loss of cohesion and loading of the arch-forming material, which is in turn caused by either a saturation of the soil by rainwater precipitation, or by the rapid draining of a submerged void, which also increases pore pressure.

(9) The geophysical data also indicated that sinkholes originated from many locations. The most hazardous area was found to be underneath resistivity profile #6 in construction site #1, with sinkholes extending over 55m and reaching depths of more than 28.7m. Another harmful area was beneath resistivity profile #6 in construction site #2, with two main depressions, one of them extending 75.0m with a maximum depth of ~15.5m, while the other extending about 55.0m with maximum depth of ~18.0 m. These features are harmful because some are in-filled with thick clay, while others are in-filled with sandy or silty clay that could collapse when situated under load, due to the weight of the structures. In

construction site #3, harmful areas were found beneath resistivity profile #4 and profile #5, with various types of sinkholes, some extending to about 15.0m to 20m, with a maximum depth of ~19.0 m. These features are harmful because some are in-filled with water, while others with thick clay and in-filled with sandy or silty clay, which could collapse when subjected to piping under load. Also, lenses with various depth and size are extended between 15.0m to75.0m, with a maximum depth of ~22.0m. Some contain thick clay, while others are in-filled with sandy or silty clay.

(10) In accordance to the characteristics of the morphological features of karstic ground conditions by (A. C. Waltham and P. G. Fookes, 2005), the karst in construction site site#1 found between profile 1 and profile 6 is an older or complex karst KIV, while the karst in construction site#2 found between profile 1 and profile 3 is a youthful karst KII. Afterwards, the karst type converted over profile#5 to profile #6 to an older, mature karst KIII. The karst in construction site#3 found between profile 1 and profile 3 is a youthful karst type KII. The karsts found profile 4 were an older, mature karst KIII, and finally, the karsts found in between profile#5 to profile#6 are older or complex karst KIV.

(11) Once the excavating work over the resistivity profile#5 was started in construction site#1, the underground water flows up straightforward; which confirms the geophysical survey that there was a source of ground water body under this profile.

## 11. Planning to mitigate the risk in construction sites developing over this carbonate karst terrain

The variety of foundation which functional for this construction sites over carbonate karst region depends upon the expect foundation loading and the degree of maturity of the karst features. The most dangerous site was this occupied to foundatings over sinkholes which affected by two controlling factors, the overloading expect and the water seep into through the cover soil.

If the problem level of construction site over carbonate karst region are known and classified, the mostly economical point of view in developing this site is to minimize the risk of structures that are founded over the area by determining the safest route in changing the plan's location. If possible, the most important part with great size and type of constructions structures has to be placed in the safest region, while the problem areas can be allocated for non-critical facilities, such as grass field, parking lots, golf courses, roadways etc.

### 11.1 The solution methods are most frequently used in the plan in order to diminish or minimize the risk of the problem areas in construction site# 1:

The first solution: Sinkhole remediation was achieved by utilizing the reverse grading technique. To fill this huge sinkhole, the hole must be excavated, and its throat plugged by concrete block, sealed with a thick grout of cement, or fill the hole with larger boulders or rocks at the bottom, followed with a cobble, then gravel or bentonite mixed with rock fragments, then sand, and finally, the top must be covered with 8-12 inches of soil. The placement of larger materials directly on the bedrock at the bottom of the sinkhole is done in order to provide support and prevent another collapse, while the smaller materials stops water from moving the soil downward into the void, and into the bedrock.

The second solution: The other solution involves drilling and driven piles down to a point where they bearing to sound rock strata then filling it with geo-graded materials to prevent the collapse of the sinkhole. If the sinkhole or cavity is dangerous to designed foundations, it must be packed with concrete, using the bridging beam to transfer the load to the side of the sinkhole.

The third solution: If it's possible, relocation the most important part with great size and type of constructions structures to be placed in the safest region, may prove to be more cost-effective in certain cases. While the problem areas can be allocated for non-critical facilities, such as grass field, parking lots.

### 11.2 The solution methods are most frequently used in the plan to diminish or minimize the risk of the problem areas in construction site# 2:

The first solution: Regular shallow spread footings and concrete grade beams to transfer the loads from the building down to the footings or piles. End-bearing piles can be driven down to transfer the structural load into soil far enough to a point where they bear on substrata bed or sound bedrock. Also skin friction piles also can be driven down so that the friction of the soil against the sides of the pile is enough to resist any downward movement.

The second solution: Soil improvement through improving the ground surface by compaction process to increase the stiffness and behaviour capacity of the soils through decreasing the permeability. Be utilized to filling the channel by using compaction grouting processes through boreholes in to the channel for the profile#1-3, to block most of the flow along particular conduits.

The third solution: Grouting by chemical solution forms, can be utilize to fill the fractures, small voids and the cavities in the subsurface layer and also in rock head pinnacles. When the solutions are injected into the cracks will seal the fractures and joints. Chemical grouting is well suited for channels, and for stabilizing

the soil around the channel for mitigating the settlement of overlying structures within the influence of the channel's configuration. Grout is injected into drilled holes along the flow paths of the channel, sealing and preventing the flow of any rainwater through them in the future.

### 11.3 The solution methods are most frequently used in the plan to diminish or minimize the risk of problem areas in construction site# 3:

The first solution: preparing the land for future development construction project, excavating and soil improvement through improving the ground surface by compaction process to increase the stiffness of the soils. Also, sinkhole remediation by using the reverse grading filter technique would be the ideal solution. To fill the small sinkholes, the bottom of the hole must be plugged with larger rocks, followed by coarse gravel, then fine gravel, coarse sand, and finally, fine sand. The upper most or final layers are bentonite clay, which prevents water seepage from occurring.

The second solution: Chemical Grouting, which is a form of penetration grouting, is a cost effective professional grouting technique that uses grouts to fill small voids in the soil with chemical solutions. The solution grouts that are commonly used include polyurethanes, acryl amides, epoxies, acrylates and sodium silicates. The soils best suited for this technique are granular soils, with significant fine sand content, that strengthen the ground and prevent excessive movement. Chemical grout is injected through the joints and gaps in the surrounding soil, where it solidifies with the soil to appear relatively impermeable and hard.

The third solution: rigid mats foundations and raft foundations, both types are known as floating foundations and are made of strongly reinforced concrete so that they can float over weaker soils. When the construction site with difficult conditions as the soil having a low bearing capacity, an economical solution of rigid mats and raft foundations types can providing the supporting to heavy structural loads. When the piles foundation cannot be used valuably and independent column footing becomes unworkable.

## 12. Recommendation

This paper describes three sites of housing complex construction projects, which are situated over a covered carbonate karst region. The hazards of the karst features were the result of mismanagement during the initial phase of the project, as the developers did not carry out prior geophysical and geological studies. Moreover, the borings within these karsts regions is incapable of providing sufficient subsurface data for analysis, and might misrepresent the subsurface geological model, which might in turn lead to additional cost for corrective design or ad-hoc analysis. The results of applying the techniques were discussed, and the recommendations are:

I.   The respective states must implement and enforce a regulation that no construction project may begin in an area over carbonate karst until the geological and geophysical survey is completed in order to avoid any future catastrophic problems.

II.  The best plan in future survey by applying (ERT) technique is using an space interval not more than 10m between two parallel lines, because of high lateral variation in the subsurface topography and lithology. Besides to give clear image to the subsurface.

III. Future survey by applying Electrical Resistivity Tomography (ERT) technique must be developed using 3D ERT survey technique and 3D software to provide a clear image for the subsurface features and structures, and also to provide clear indications of their directions and extent under the subsurface.

IV.  Using the borings method to support the result of the (ERT) techniques survey to position early plans that minimizes the hazard of karst features in any construction sites over covered karstified carbonate bedrock before the start of the project.

## 13. Conclusion

This paper focuses on the application of Electrical Resistivity Tomography (ERT), aerial photographs, and satellite images as identification techniques for geohazard assessment of karst features across three construction sites of housing complex of north Ipoh city, Perak, peninsular Malaysia.

Two-dimensional (2-D) electrical resistivity imaging/tomography surveys are carried out by employing a large number of electrodes; 41, 61 and 81 electrodes along straight lines over three construction sites. Construction site #1 is located at Klebang Putra – Klebang Green, and Construction site #2 is located at Medan Klebang Restu-Klebang Damai, while Construction site #3 is located north Bandar Baru Putra, the main road to Tanjung Malim, north of Ipoh, Perak, Peninsular Malaysia.

The ERT technique was applied in this geo-technical survey to investigate karst features, such as sinkholes, cavities, depressions and channel pipes, due to the fact that the tool is suitable for differentiating surficial soil, clay, sand, weathered marbleized limestone bed rocks, intact marbleized limestone bed rocks, water - air-filled cavities, and channels. The simplicity of its application was also a major factor in its application decision. It is based on the application of electric current into analyzed bedrock and measuring the intensity of electrical resistivity to its conduit. Basically, it provides information of electrical resistivity properties through the

analyzed material towards the electrical current passage.

An assessment of the situation was surmised from the subsurface images. Subsequently, an estimation of the possibility of a collapse occurring due to the sinkhole was prepared. The explanation of the geophysical data reveals that both very low resistivity and high conductivity abnormalities extend along the projected areas into the construction sites. The emergence of many famous sinkholes in the affected section is regularly accredited to karstic activities. Also, the geophysical data indicated that the depth of the limestone bedrock was asymmetrical or uneven, containing many pinnacles and cutters, so the borings within this karsts regions do not overlap the area concerned on the subsurface, and is incapable of providing sufficient subsurface data for analysis, and at the same time, might also misrepresent the subsurface system, which may lead to additional costs for corrective design or additional analysis.

The karst structure level in construction site#1 found between profile 1 and profile 6 is an older or complex karst type KIV, while the karst in construction site#2 found between profile 1 and profile 3 is a youthful karst type KII. Afterwards, the karst type changed over profile#5 to profile #6 to mature into karst type KIII. The karst in construction site#3, found between profile 1 and profile 3, is a youthful karst type KII. Then, the karsts changed in profile 4 to an older, mature karst type KIII. The karsts found between profiles #5 to profile#6 are of the older or complex karst type KIV. Consequently, early planning is required to minimize the risk to structures in these construction sites over covered karstified carbonate bedrock. Initial consolidation of reverse geo grading technique, driven piles to rock head pinnacles, chemical grouting and control the drainage works must be put into operation at these sites.

**References**

A. C. Waltham1 and P. G. Fookes, 2005, engineering classification of karst ground conditions, Quarterly Journal of Engineering Geology and Hydrogeology, v. 36, p. 101-118.

Dahlin T., 1996, 2D resistivity surveying for environmental and engineering applications, First Break, v. 14(7), p. 275-283.

Gobbett, D.J. 1964. The Lower Paleozoic Rocks of Kuala Lumpur, Malaysia. Federation Museum's Journal, 9, 67-79.

Hoover R. A. and Saunders W.R., 2000, Evolving Geophysical Standards, in Proceedings, The First International Conference on the Application of Geophysical Methodologies & NDT to Transportation Facilities and Infrastructure Conference Proceedings, Missouri Department of Transportation.

Hussein, I. E., Kraemer, G. and Myers, R., 2000,Geophysical characterization of a proposed street extension in Cape Girardeau, Missouri, in Proceedings, The First International Conference on the Application of Geophysical Methodologies & NDT to Transportation Facilities and Infrastructure.

Hutchinson, C.S., 2007. Geological Evolution of South-East Asia (2nd Edition), Geological Society of Malaysia (Publ), 433 p.

Ingham, F.T. and E.P. Bradford, 1960.The geology and mineral resources of the Kinta Valley, Perak. Geological Survey District Memoir 9, Federation of Malaya Geological Survey, Ipoh, 347 p.

Ingham, F.T. and E.P. Bradford, 1960.The geology and mineral resources of the Kinta Valley, Perak. Geological Survey District Memoir 9, Federation of Malaya Geological Survey, Ipoh, 347 p.

Ioannis F. Louis, Filippos I. Louis and Melanie Bastou, 2002, Accurate Subsurface Characterization For Highway Applications Using Resistivity Inversion Methods, Geophysics & Geothermic Division, Geology Department, University of Athens, Panepistimiopolis,Ilissia, Athens.

Loke, M. H. and Barker, R. D. 1994. Rapid least-squares inversion of apparent resistivity pseudo-sections, Extended Abstracts of Papers 56thEAGE Meeting Vienna, Austria 6-10 June 1994, p. 1002.

Loke, M.H., 1994, The inversion of two-dimensional resistivity data. Unpubl., PhD thesis, University of Birmingham.

Loke, M.H., 1999, Time-lapse resistivity imaging inversion, in Proceedings, 5th Meeting of the Environmental and Engineering Geophysical Society European Section, Em1.

Muhammad, R. F, 2003, The Characteristic and Origin of the Tropical Limestone Karst of the Sungai Perak Basin, Malaysia, Unpubl. PhD, University of Malaya, p. 443

Muhammad, R. F. &Yeap, E. B. 2002, Estimating Dissolution Rates in Kinta and Lenggong Valleys the Micro Erosion Meter, Geol Soc Bull. V. 45, p. 26-27.

Neil L. Anderson, Derek B. Apel and Ahmed Ismail, 2007, Assessment of Karst Activity at Highway Construction Sites Using the Electrical Resistivity Method, Missouri, USA.

Niel A. Yahia, Yassin R. Rafeeq,Samer R. Hujab , 1993, The application of complex geophysical techniques to detecting and locating the Weakness zone and the water seepage in the body of the AL-

Tharthar dam , Samara Town, Salahuddin province, Iraq geosurv, Baghdad – Iraq, NI-38-10,SEGSM, 2265.

Psomiadis David , Tsourlos Panagiotis, Albanakis Konstantinos, 2008,Electrical resistivity tomography mapping of beach rocks, application to the island of Thassos (N. Greece), Environ Earth Sci (2009), v. 59:233–240, DOI 10.1007/s12665-009-0021-9.

Reitz, H.M., and Eskridge, D.S., 1977, Construction methods which recognize the mechanics of sinkhole development, in Dilamarter, R.R., and Csallany, S.C., eds., Hydrologic problems in karst regions: Bowling Green, Western Kentucky University, Department of Geology and Geography, p. 432-438.

Sowers, G.F., 1996, Building on sinkholes: Design and construction of foundations in karst terrain: American Society of Civil Engineers, New York, p. 115.

Telford, W.M., Geldart, L.P., and Sheriff, R.E., 1990, Applied Geophysics, (2nd add).  Cambridge University Press, New York.

W. Zhou 7 B.F. Beck 7 J.B., 2000, Stephenson Reliability of dipole-dipole electrical resistivity tomography for defining depth to bedrock in covered karst terrains.

William E. Doll', Jonathan E. Nyquist2, Philip J. Carpenter3, Ronald D.Kaufmann4, and Bradley J. Car-r', 2002, Geophysical Surveys of a Known Karst Feature, Oak Ridge Y-12 Plant, Oak Ridge, Tennessee .

Yahia, Nail Abdel Al-Qadir, Yassin, Riyadh Rafeeq, Abdel Al-Qadir, Sabah Omar, 1994, The results of Application of geophysical Techniques in the exploration of Bauxites Ore deposits in subsurface karsts terrains, Iraqi Western Desert,  Rep.no2262,geosurv, Baghdad – Iraq.

Yassin,  Riyadh R, Hj Taib Samsudin, Muhammad Ros Fatihah,2013, Reliability of Wenner ER Tomography and satellite image techniques in recognizing and assessing the geohazard development of subsurface carbonate karst features in selected construction sites in (Kinta valley) Perak, Peninsular Malaysia, The fifth AUN/SEED-Net regional conference on Geological Engineering, Kuala Lumpur, Malaysia.ISBN:978-967-0380-23-0.

Yassin, Riyadh Rafeeq, 2002, evaluates the presence of karstic Bauxitic clay deposits in parts of western desert of Iraq by the application of VLF – electromagnetic and Electrical resistivity techniques, MsC thesis submitted to Department of Geology, college of science, university of Baghdad, p. 293.

**First Author**, Riyadh R. Yassin, Born in Baghdad, Iraq. BsC in geophysics, MsC 2001-2002, in "applying geophysical techniques in mineral exploration", University of Baghdad, Iraq. PhD candidate in 2008-2009, university of Malaya, Kuala Lumpur, Malaysia. Senior chief of geologist 2006, in (geosurv. Iraq). The major field of work and study is geo-engineering, mineral exploration in karst terrains.  Member of Iraqi Geologist Union (1990).  Member of Geological Society of Malaysia (2008). Member of Natural Society of Malaysia (2009).